

SiMPLISTIC: A Novel Pairwise Potential for Implicit Solvent Lipid Simulations with Single-site Models

Somajit Dey*, Jayashree Saha

Department of Physics, University of Calcutta, 92, A.P.C. Road, Kolkata-700009, India

Last Modified: October 5, 2020

ABSTRACT

Implicit solvent, coarse-grained models with pairwise interactions can access the largest length and time scales in molecular dynamics simulations, owing to the absence of computationally expensive interactions with a huge number of solvent particles, the smaller number of interaction sites in the model molecules, and the lack of fast sub-molecular degrees of freedom. Without an explicit solvent, the solvent mediated effects, e.g. the hydrophobic effect and the hydration force, are mimicked entirely through the interactions between the model molecules. In this paper, we describe a maximally coarse-grained model for lipids in implicit water. The model is called SiMPLISTIC, which is an acronym for ‘Single-site Model with Pairwise interaction for Lipids in Implicit Solvent with Tuneable Intrinsic Curvature’. SiMPLISTIC lipids rapidly self-assemble into realistic non-lamellar and lamellar phases such as inverted micelles and bilayers, the spontaneous curvature of the phase being determined by a single free parameter of the model. Model membrane simulations with lamellar SiMPLISTIC lipids show satisfactory fluid and gel phases with no interdigitation or tilt. Despite being rigid molecules, SiMPLISTIC lipids can generate experimentally relevant values for the bending stiffness of model membrane bilayers with no significant interleaflet coupling. SiMPLISTIC can also simulate mixtures of lipids that differ in their packing parameter or length, the latter leading to the phenomenon of hydrophobic mismatch driven phase separation or domain formation. The model has a large scope due to its speed, conceptual and computational simplicity, and versatility. Applications may range from academic and industrial research in various lipid-based systems, such as lyotropic liquid crystals, biological and biomimetic membranes, vectors for drug and gene delivery, emulsions for cosmetic products, to education, such as teaching/learning concepts like self-assembly, polymorphism, biomembrane organization etc. through interactive molecular dynamics simulations.

KEYWORDS

Coarse-graining; Lipid polymorphism; Implicit-solvent; Molecular dynamics; Self-assembly; Lyotropic liquid crystals

I. INTRODUCTION

Lipids are amphiphiles, usually consisting of a hydrophilic polar headgroup linked to two hydrophobic hydrocarbon chains (tails)¹. Amphiphiles, based on their effective molecular shape or packing parameter², self-assemble in aqueous dispersions into phases with different morphologies³. Lipids, likewise, also show polymorphism in aqueous dispersions^{1,4}. The rather unusual single chain lysolipids form micelles⁵. Lipids with saturated alkyl chains and those with unsaturated chains but bigger headgroups form lamellar bilayers (gel or fluid)^{6,7}. Lipids with smaller headgroups, including cholesterol¹, on the other hand, form various non-lamellar phases with negative curvatures such as inverted or reversed micelles, inverted hexagonal and bicontinuous cubic phases⁸. Non-lamellar phases with positive curvatures, however, are uncommon in lipid polymorphism¹. By non-lamellar phases in the following, therefore, we shall refer to non-lamellar phases with negative curvatures only.

Both lamellar and non-lamellar phase forming lipids are important in natural biology as well as biomedical and industry applications. The cell membrane, for example, contains both lamellar and non-lamellar lipids⁹. The non-lamellar lipids tune the membrane curvature and are predominantly present in the cytosolic leaflet^{10,11}. Non-lamellar lipids also find applications in drug delivery¹², gene therapy¹³ and cosmetics formulations¹⁴. Lamellar lipids are widely studied in the contexts of natural biology¹⁵, biomimetics¹⁶, biomedical^{17,18} and cosmetic applications¹⁹.

The physics of lipids in water is multiscale – both spatially and temporally – and involves cooperative phenomena. Such many-body, multiscale physics is best probed using computer simulations. Besides complementing experiments quantitatively, molecular simulations can provide significant qualitative insights into the structure, function and dynamics of lipid aggregates⁷. Simulations can also decide between competing continuum theories or even guide experiments²⁰.

The level of detail in a molecular simulation model practically determines the scale accessible by the simulation. The higher the model resolution, the smaller is the timescale or system size that can be simulated. Even with the current state-of-the-art in high performance computing (viz. massively parallel processing and GPU acceleration) bridging the nanoscale atomistic dynamics to large-scale phenomena such as self-assembly, domain formation, membrane fusion etc. that span micrometers in length and milliseconds in time, is still a far cry for all-atom classical molecular dynamics (MD) simulations²¹. Consequently, some level of coarse-graining (CG) is needed in the models, which trades the full atomic level resolution of an all-atom

approach for a unified atom or a molecular level representation. The various approaches to CG modeling of biomolecular systems and solvated amphiphiles are well-discussed in the literature and the reader is referred to Ref. 22 and 23 for excellent overviews on the topic.

Of the different CG methodologies used for modeling lipids in water, a special class consists of implicit solvent, top-down approaches in which the lipids are modeled as single or multisite molecules interacting via ad hoc potentials that are designed for simplicity and speed of computation. ‘Implicit solvent’^a means water is never modeled explicitly, the solvent effects being incorporated within effective interactions between lipids. Any vacuum or unoccupied space in the simulation box, therefore, should be considered as water (Figure 1). These particle-based models are top-down in the sense that they are supposed to reproduce the mesoscopic and macroscopic properties such as self-assembly, membrane elasticity etc. without considering the microscopic details explicitly. An accessible review of such implicit solvent coarse-grained (ISCG) models can be found in Ref. 24.

The goal of the present paper is to present a novel ISCG model for self-assembling lipids, where the lipids are modeled as single-site directed ellipsoids interacting via a simple, two-body, anisotropic potential. Being molecular level (i.e. single-site) and implicit solvent, the number of site-site interactions is minimal and the MD timestep can be maximum, because of which this model can simulate lipid systems at the largest scales accessible by any particle-based model for given computational resources. The pairwise interaction potential features a tuneable parameter that determines the spontaneous curvature of the self-assembled phase. For ease of reference, we shall henceforth call this model ‘SiMPLISTIC’, which is an acronym for ‘Single-site Model with Pairwise interaction for Lipids in Implicit Solvent with Tuneable Intrinsic Curvature’.

To put SiMPLISTIC in perspective, let us briefly discuss some of the previous attempts at minimalistic,^b ISCG modeling of lipids for off-lattice simulations. The pioneering model by Drouffe et al.²⁵ consisted of directed spheres, which, using a multibody hydrophobic potential, self-assembled into monolayers. To simulate a lipid bilayer with this monolayer, each sphere would be viewed as containing a hydrophobic layer sandwiched between two (top and bottom) hydrophilic layers. This model, therefore, represented a pair of lipids instead of a single

^a Some authors use the term ‘Solvent-free’ instead.

^b By ‘minimalistic’, we mean models with up to three interaction sites only. For other ISCG models see Ref. 48,49,80–82 and the references therein.

lipid. Nogushi and Takasu²⁶ were the first to give an ISCG model of a single lipid proper. Their model consisted of a rigid, linear trimer of one hydrophilic and two hydrophobic beads. Self-assembly was still due to a multibody hydrophobic potential. Pairwise potentials, however, are far more computationally efficient than multibody ones. This led to the ‘Water-free’ model by Farago²⁷ where each lipid was still modeled as a rigid, linear trimer, but now all interactions were pairwise. Brannigan and Brown²⁸ took a different approach and brought nonspherical components into the picture. Their model consisted of a nematogenic spherocylinder with a hydrophobic site at its one end, all interactions being pairwise. The molecules in the four models mentioned above are essentially rigid linear rotors with only five degrees of freedom. The fluid bilayers produced by them, however, were either too flexible (forming vesicles easily)^{25,26} or too stiff (comparable to membranes with cholesterol)^{27,28}. To remedy this, Wang and Frenkel²⁹ introduced flexibility in the bead-based trimer model by using finite extensible nonlinear elastic (FENE) bonds to link the beads. By this time, it had already become clear for the workers in this field that simple Lennard-Jones (LJ) potentials are not suitable for stabilizing a fluid bilayer. To this effect, some had to use density-dependent multibody potentials^{25,26,29} and some²⁸ employed anisotropic, inverse-squared attraction with a longer interaction range. Although Farago²⁷ was able to stabilize a fluid bilayer with LJ type interactions only, he had to make the pair potentials non-additive and remain limited to only a heavily tuned set of parameters. Farago’s strategy required the hydrophobic beads to see the hydrophilic beads as larger than they actually were, thus creating a steric barrier against lipid evaporation from the membrane plane. As expected, this compromised self-assembly and only preassembled bilayers could be studied. Cooke, Kremer and Deserno^{30,31} then realized the capability of broad attractive tail potentials to accomplish self-assembly into stable fluid bilayers. Their model³⁰ was again a flexible (FENE linked) trimer with the hydrophobic beads attracting each other pairwise and the hydrophilic beads providing soft-core, steric interaction only. The range of the pairwise attraction, however, was now a tuneable parameter that affects the thermal stability and the elasticity of the bilayer. For completeness, we must mention the relatively recent model by Noguchi³², where each lipid is modeled as a directed sphere with two interaction sites and self-assembly is ensured using a multibody hydrophobic potential.

A notable commonality between the above-mentioned ISCG models with pairwise interactions is that none of them incorporates the hydration force³³, which is a key feature of hydrated amphiphile aggregates. Hydration force accounts for the effective repulsion between two hydrophilic layers in close contact, and decays exponentially with the distance between them. This ‘hydration barrier’ is the reason, apart from thermal fluctuations such as protrusions and undulations, why membrane fusion is difficult³⁴ and why a bilayer cannot sit immediately on top of another in multilamellar stacks^c (Figure 1a). In 2017, we published a single-site, ISCG model for amphiphiles, with a pairwise, anisotropic potential, that could mimic such a ‘hydration barrier’.³⁵ Amphiphiles were modeled as soft-core directed spheroids that attracted each other, mimicking hydrophobic force, for some relative orientations and repelled each other, mimicking hydration force, for the rest. Because of this, the packing parameter of the molecule could become that of a (truncated) cone even though the steric core was ellipsoidal. The model featured two key parameters: a tuneable range parameter as in the Cooke-Kremer-Deserno model³⁰, and a packing parameter tuner that would determine the aggregate morphology. Unlike the rigid anisotropic models of Brannigan and Brown²⁸ and Noguchi³², our single-site 2017 model required no exclusively hydrophobic or hydrophilic interaction site, and yet showed rapid, unassisted self-assembly into fluid bilayers, rods and micelles. As a further test of this model, we used it to build ISCG models of both rigid and flexible bolaamphiphiles³⁶, which successfully reproduced many key features of hydrated bolaamphiphile systems in MD simulations.

^c Adding water to an anhydrous multilamellar stack introduces a layer of water between consecutive bilayers which leads to ‘swelling’⁸³.

Although this 2017 model³⁵ fulfilled our requirement of a computationally fast, conceptually and programmatically simple^d ISCG model for generic amphiphiles with various packing parameters, it could not generate phases with negative curvatures. Hence, we could not use it to model the non-lamellar lipids. In fact, to the best of our knowledge, none of the above-mentioned minimalistic ISCG models had been shown to produce stable aggregates with negative intrinsic curvatures through spontaneous self-assembly. This is not surprising when we recognize that the formation of inverted morphologies by ISCG models is more involved than merely getting the molecular packing parameters right. To illustrate, an obvious difference between an inverted micelle with its negative curvature and a direct micelle with positive curvature is that the direct micelle does not encapsulate water whereas the inverted micelle does (Figure 1b and c). The hydration barrier due to this captured water should therefore be taken into account appropriately in an implicit solvent model and a simple model that mimics only the packing parameter of the lipids would not suffice^e. This is where our new ISCG model SiMPLISTIC fits in. Here, the model particles can efficiently self-assemble into inverted micelles that encapsulate vacuum, which is to be interpreted as water because the model is implicit solvent. SiMPLISTIC can also form bilayers. It can therefore model both lamellar and non-lamellar lipids. In addition, for model membranes, SiMPLISTIC can generate elastic properties consistent with experiments and other simulations, unlike the other rigid models (see discussion [above](#)). Other important features implemented in SiMPLISTIC are the hydrophobic mismatch between lipids of unequal lengths for studying demixing and domain formation in multicomponent membranes, mixing rules for studying mixtures of lamellar and non-lamellar lipids, and the ability to form interdigitation-free bilayers regardless of the lipid length. The latter is relevant in view of the fact that phospholipids with symmetric acyl chain lengths do not show interdigitation in bilayers.

SiMPLISTIC, to the best of our knowledge, is the first, truly single-site model for self-assembling lamellar and non-lamellar lipids using a pairwise potential. SiMPLISTIC’s ability to model non-lamellar lipids by simply tuning a parameter, however, came as a by-product. Our original scheme was to design the most minimalistic, single-site lipid model for large-scale model membrane simulations with pairwise interactions only. The basic aim, therefore, was to be able to generate fluid, interdigitation-free bilayers through rapid, spontaneous self-assembly, while also taking into account the interbilayer hydration force. The next section (Sec. II) presents the design of SiMPLISTIC with this original purpose in mind. Sec. III then discusses how the ability to self-assemble into aggregates with different curvatures comes along because of our chosen pair potential. Finally, Sec. IV reports the results of model membrane simulations and extends SiMPLISTIC to include hydrophobic mismatch between lipids of different lengths. We conclude this paper in Sec. V with discussions of SiMPLISTIC’s speed, scope and future directions.

II. THE MODEL: SiMPLISTIC

A. Design Principles

Given the ad hoc nature of any top-down, ISCG model, it is necessary to lay down a set of design principles around which the model would be developed. If certain design principles lead to a successful model, then those principles must have captured some essence of the physics involved at the time and length scales appropriate to the model. The design of SiMPLISTIC is based on the following core principles.

^d The model potential was essentially a (switched) Gay-Berne potential⁴⁰ with a modified well-depth and a broad (cubic spline) tail.

^e For example, no non-lamellar, inverted phase such as the inverted hexagonal, micellar or cubic phase was formed by the Cooke-Deserno model, even when the lipid profile was made inverted conical by making the headgroup bead smaller than the hydrophobic beads⁸⁴.

1. Absence of sub-molecular degrees of freedom

We choose a rigid model. This makes the model molecule translate and rotate as a whole with a timescale that is larger than the sub-molecular degrees of freedom of a flexible molecule would ever allow. A rigid model, therefore, can have the largest MD timestep. Other works in the literature have also found the use of rigid models fruitful^{27,28,32,35,37}. Using ³¹P-NMR data and MD simulations, Klauda et al.³⁸ established the rigid body modeling to be a good description of phospholipids in a fluid bilayer. Lipids could be viewed as rigid cylinders with two primary modes of rotation – rotation about the long axis and wobble. According to Marsh³⁹, rapid long axis rotation kicks in by the main transition. This motivates an axisymmetric model of lipids for our case. Because the lipids are not inversion symmetric, a rigid model of lipids must also have an inherent directedness that may be described by a unit vector $\hat{\mathbf{u}}$ directed from the tail end to the head end (see inset of Figure 2). Such an axisymmetric and directed model has only five physically significant degrees of freedom, viz. the orientation of its unit vector and its centre of mass (c.m) coordinates. The remaining degree of freedom, viz. the rotation about its axis of symmetry is physically inconsequential.

2. Single-site model with pairwise interaction

A valid single-site model with a simple, anisotropic pair potential is both economic and elegant compared to an equally valid model with multiple interaction sites, if both the models are to be applied at the same length and time scales. The legacy of the Gay-Berne potential (GB) has been particularly influential in this context. GB⁴⁰ is a simple, single-site, anisotropic potential that was originally designed to substitute for a rigid tetramer of LJ sites, and has since seen remarkable popularity in modeling mesogenic molecules in liquid crystal research^{41–43}.

3. Template for the pair potential

Let us take two model particles i and j with c.m coordinates \mathbf{r}_i and \mathbf{r}_j and unit vectors $\hat{\mathbf{u}}_i$ and $\hat{\mathbf{u}}_j$ respectively. The distance between the c.m is denoted by $r = |\mathbf{r}_{ij}|$, where $\mathbf{r}_{ij} = \mathbf{r}_i - \mathbf{r}_j$. The generic form of a soft-core, pair potential between them can now be written in the well-known Weeks-Chandler-Anderson^{44,45} format as

$$V_{ij} = V_{ij}^{\text{Repulsive}} + V_{ij}^{\text{Attractive}}, \quad (1)$$

where

$$\begin{aligned} V_{ij}^{\text{Repulsive}} &= V^{\text{Steric}}(r) \text{ if } r < r_{zf} \\ &= 0, \text{ otherwise} \end{aligned} \quad (2)$$

and

$$\begin{aligned} V_{ij}^{\text{Attractive}} &= -\epsilon_{\text{wd}}, \text{ if } r < r_{zf} \\ &= s(r)\epsilon_{\text{wd}}, \text{ if } r_{zf} \leq r < r_{\text{cut}} \\ &= 0, \text{ otherwise} \end{aligned} \quad (3)$$

Meanings of the variables used above are the following. r_{zf} : r at which the potential is minimum and the particles exert zero force on each other; r_{cut} : r at which the potential decays to zero or is cut-off; ϵ_{wd} : the well-depth of the attractive potential; $s(r)$: a spline curve that switches from -1 at r_{zf} to 0 or near zero at r_{cut} ; $V^{\text{Steric}}(r)$: A strictly repulsive potential describing the soft-core. Contextually, it might be noted that the popular LJ and GB potentials also comply with the format given in Eq. (1)-(3). As in GB, any anisotropy in the pair potential is introduced through the dependence of r_{zf} and ϵ_{wd} on the relative orientation of the particles. $r_{zf}(\hat{\mathbf{r}}_{ij}, \hat{\mathbf{u}}_i, \hat{\mathbf{u}}_j)$, for example, would correspond to the nonspherical shapes of the molecular cores.

Desirably, the pair potential should be symmetric under swapping of the particles, viz. $V_{ij} = V_{ji}$. For an anisotropic potential, this implies that the functions $\epsilon_{\text{wd}}(\hat{\mathbf{r}}_{ij}, \hat{\mathbf{u}}_i, \hat{\mathbf{u}}_j)$ and $r_{zf}(\hat{\mathbf{r}}_{ij}, \hat{\mathbf{u}}_i, \hat{\mathbf{u}}_j)$ should depend only on terms symmetric in i and j . Some of the simplest examples of such terms are $(\hat{\mathbf{u}}_i \cdot \hat{\mathbf{u}}_j)$, $(\hat{\mathbf{r}}_{ij} \cdot \hat{\mathbf{u}}_i + \hat{\mathbf{r}}_{ji} \cdot \hat{\mathbf{u}}_j)$ and $(\hat{\mathbf{r}}_{ij} \cdot \hat{\mathbf{u}}_i)(\hat{\mathbf{r}}_{ji} \cdot \hat{\mathbf{u}}_j)$. The directedness or inversion asymmetry of the lipids also requires $\epsilon_{\text{wd}}(\hat{\mathbf{r}}_{ij}, \hat{\mathbf{u}}_i, \hat{\mathbf{u}}_j) \neq \epsilon_{\text{wd}}(\hat{\mathbf{r}}_{ij}, -\hat{\mathbf{u}}_i, -\hat{\mathbf{u}}_j)$.

4. Phenomenology

Being top-down, our ISCG modeling approach needs to be guided by some phenomenology of generic lipid bilayers. A preference for certain relative configurations between a pair of nearest neighbor lipids in a hydrated bilayer can be easily ascertained from the schematic in Figure 1a. The lipids labeled 1 and 2 are in the side-side parallel (SSP) configuration, whereas those labeled 1 and 3 are in the tail-tail collinear (TTC) configuration. In a stable bilayer, lipids 1, 2 and 3 are bound to each other. If all the lipids interact only through an implicit solvent pair potential as described in Sec. II.A.3, this implies that the SSP and TTC configurations must have negative pair potential energies or, equivalently, positive well-depths (ϵ_{wd}).

Lipids 1 and 4 in Figure 1a, on the other hand, belong to adjacent bilayers. They, therefore, should repel each other in their head-head collinear (HHC) configuration so as to mimic the effective hydration force between those bilayers. The potential described in Eq. (3), therefore, needs to be repulsive for the HHC configuration, which is possible if $\epsilon_{\text{wd}}^{\text{HHC}} < 0$.

Figure 2 lists all possible side-side and collinear configurations between a pair of model lipids. For the sake of discussion, we shall call these the canonical configurations. Let us now discuss the remaining two canonical configurations that we did not discuss before. If a lipid in a bilayer leaflet is flipped upside down about its centre of mass, it will give rise to the side-side antiparallel (SSA) and the head-tail collinear (HTC) configurations as shown in Figure 3a. Because such a flip is prohibited, as otherwise it would expose the flipped lipid's tail to the surrounding water, the SSA and HTC configurations must be highly unstable. Lipid pairs in SSA or HTC configurations, therefore, must be unbound, which, like the HHC case above, requires $\epsilon_{\text{wd}}^{\text{SSA}} < 0$ and $\epsilon_{\text{wd}}^{\text{HTC}} < 0$. Making the SSA and HTC configurations unfavorable, contributes to bilayer stability in other ways too. To illustrate, note that the SSA configuration also arises in case of extreme interleaflet interdigitation, viz. when the lipids from one leaflet are pushed into the other leaflet, thus thinning the bilayer down to the width of a monolayer (Figure 3b). In order to avoid the unstable SSA configuration, therefore, the leaflets start to push each other away. This way, the model monolayers can produce a realistic resistance when forced to interdigitate. On the other hand, when a lipid protrudes out of the bilayer plane or tries to escape from the bilayer, it must pass through a configuration where its tail comes near the head of the neighboring lipids, all the lipids being parallel (Figure 3c). This configuration is very close to HTC and hence, must be unstable. Consequently, the bilayer remains stable against lipid protrusion and evaporation, as desired.

So far, we have decided only on the signs of ϵ_{wd} for the canonical configurations listed in Figure 2 by considering their stability or instability. Thermodynamic reasoning enables us to go further. Let T_{fluid} denote the physiological temperature at which the model lipid bilayer must remain stable and fluid. Because r_{cut} is finite, this requires each of the intraleaflet and interleaflet nearest neighbor pairwise binding energies to be comparable in order of magnitude to the thermal energy, viz. $O(\epsilon_{\text{wd}}^{\text{SSP}}) \approx O(\epsilon_{\text{wd}}^{\text{TTC}}) \approx O(kT_{\text{fluid}})$, where k denotes the Boltzmann constant. In addition, to ensure stability against thermally induced leaflet interdigitation as well as lipid protrusion and evaporation, and to enforce the interbilayer hydration barrier, we require the three unbound canonical configurations to have sufficient

potential energy barrier at the physiological temperature.
Eq. (4) summarizes our conclusions for later reference.

$$\begin{aligned} \varepsilon_{\text{wd}}^{\text{SSP}}, \varepsilon_{\text{wd}}^{\text{TTC}} > 0, \quad \varepsilon_{\text{wd}}^{\text{HHC}}, \varepsilon_{\text{wd}}^{\text{SSA}}, \varepsilon_{\text{wd}}^{\text{HTC}} < 0 \\ O(\varepsilon_{\text{wd}}^{\text{SSP}}) \approx O(\varepsilon_{\text{wd}}^{\text{TTC}}) \approx O(kT_{\text{fluid}}) \\ O(-\varepsilon_{\text{wd}}^{\text{HHC}}), O(-\varepsilon_{\text{wd}}^{\text{SSA}}), O(-\varepsilon_{\text{wd}}^{\text{HTC}}) \geq O(kT_{\text{fluid}}) \end{aligned} \quad (4)$$

B. Model Definition

In view of Sec. II.A.3, to define SiMPLISTIC completely, we only need to specify the steric profile, viz. $V^{\text{Steric}}(r)$ and $r_{\text{zf}}(\hat{\mathbf{r}}_{ij}, \hat{\mathbf{u}}_i, \hat{\mathbf{u}}_j)$, the anisotropic well-depth $\varepsilon_{\text{wd}}(\hat{\mathbf{r}}_{ij}, \hat{\mathbf{u}}_i, \hat{\mathbf{u}}_j)$, and the tail $s(r)$.

1. Steric profile

Mesogenic molecules are frequently modeled as uniaxial, elongated, rigid objects in liquid crystal simulations, and two simplest shapes normally chosen to represent the shape of the molecular cores⁴³ are— a) the spherocylinder and b) the Gay-Berne spheroid^f. The spherocylinder is more efficient for Monte-Carlo (MC) simulations, whereas the GB spheroid is better suited for Molecular Dynamics (MD). This is because, although the contact distance (or distance of closest approach) is simpler to compute for the spherocylinder⁴⁶, the computation of the gradients of the contact distance as required for force and torque determination in MD is far cheaper for the GB spheroid⁴⁷. Because our research group uses MD exclusively, we chose the GB spheroid for the core of SiMPLISTIC.^g

For a GB spheroid of width σ_0 and length σ_e , the contact distance is given as

$$\begin{aligned} \sigma_{\text{GB}}(\hat{\mathbf{r}}_{ij}, \hat{\mathbf{u}}_i, \hat{\mathbf{u}}_j) &= \sigma_0 \left[1 - \frac{\chi}{2} \left\{ \frac{(\hat{\mathbf{r}}_{ij} \cdot \hat{\mathbf{u}}_i + \hat{\mathbf{r}}_{ij} \cdot \hat{\mathbf{u}}_j)^2}{1 + \chi(\hat{\mathbf{u}}_i \cdot \hat{\mathbf{u}}_j)} + \frac{(\hat{\mathbf{r}}_{ij} \cdot \hat{\mathbf{u}}_i - \hat{\mathbf{r}}_{ij} \cdot \hat{\mathbf{u}}_j)^2}{1 - \chi(\hat{\mathbf{u}}_i \cdot \hat{\mathbf{u}}_j)} \right\} \right]^{-1/2} \\ &= \sigma_0 \left[1 - \frac{\chi \left[(\hat{\mathbf{r}}_{ij} \cdot \hat{\mathbf{u}}_i)^2 + (\hat{\mathbf{r}}_{ji} \cdot \hat{\mathbf{u}}_j)^2 \right] + 2\chi^2 (\hat{\mathbf{r}}_{ij} \cdot \hat{\mathbf{u}}_i)(\hat{\mathbf{r}}_{ji} \cdot \hat{\mathbf{u}}_j)(\hat{\mathbf{u}}_i \cdot \hat{\mathbf{u}}_j)}{1 - \chi^2 (\hat{\mathbf{u}}_i \cdot \hat{\mathbf{u}}_j)^2} \right]^{-1/2} \end{aligned} \quad (5)$$

The anisotropy parameter χ is related to the aspect ratio $\sigma_0 : \sigma_e$ of the spheroid as $\chi = [(\sigma_e / \sigma_0)^2 - 1] / [(\sigma_e / \sigma_0)^2 + 1]$. Following the soft-core, repulsive part of the GB potential⁴⁰, let us now define $V^{\text{Steric}}(r)$ for SiMPLISTIC as

$$V^{\text{Steric}}(r) = 4\varepsilon_0 \left(\frac{1}{R^{12}} - \frac{1}{R^6} \right) + \varepsilon_0, \quad (6)$$

where $R = (r - \sigma_{\text{GB}} + \sigma_0) / \sigma_0$ and ε_0 serves as an energy scale for the model interaction strength. r_{zf} for the above-defined $V^{\text{Steric}}(r)$ is at $r = (2^{1/6} - 1)\sigma_0 + \sigma_{\text{GB}}$.

2. The tail of the model potential

Deserno and coworkers clearly demonstrated the efficacy of a broad attractive tail potential for generating fluid bilayers through self-assembly³¹. In our 2017 amphiphile model³⁵ and our subsequent work on bolas³⁶, we too showed successful self-assembly, using a simple

cubic spline as the broad attractive tail^h. In the same vein, $s(r)$ for SiMPLISTIC is now defined as

$$s(r) = (r_{\text{cut}} - r)^2 (3r_{\text{zf}} - 2r - r_{\text{cut}}) / (r_{\text{cut}} - r_{\text{zf}})^3. \quad (7)$$

Note that the difference $r_{\text{cut}} - r_{\text{zf}}$ determines the range of pairwise attraction for attractive configurations like SSP and TTC and the range of hydration barrier for HHC. This difference is therefore a parameter of SiMPLISTIC which we shall call *range*.

3. Well-depth

In view of the discussion in the last paragraph of Sec. II.A.3, we shall try to form $\varepsilon_{\text{wd}}(\hat{\mathbf{r}}_{ij}, \hat{\mathbf{u}}_i, \hat{\mathbf{u}}_j)$ using the terms $(\hat{\mathbf{u}}_i \cdot \hat{\mathbf{u}}_j)$, $(\hat{\mathbf{r}}_{ij} \cdot \hat{\mathbf{u}}_i + \hat{\mathbf{r}}_{ji} \cdot \hat{\mathbf{u}}_j)$ and $(\hat{\mathbf{r}}_{ij} \cdot \hat{\mathbf{u}}_i)(\hat{\mathbf{r}}_{ji} \cdot \hat{\mathbf{u}}_j)$. Note that these three terms are also sufficient to distinguish between all the canonical configurations in Figure 2. This is illustrated in Table 1 below.

Term	SSP	TTC	SSA	HTC	HHC
$(\hat{\mathbf{u}}_i \cdot \hat{\mathbf{u}}_j)$	1	-1	-1	1	-1
$(\hat{\mathbf{r}}_{ij} \cdot \hat{\mathbf{u}}_i + \hat{\mathbf{r}}_{ji} \cdot \hat{\mathbf{u}}_j) / 2$	0	1	0	0	-1
$(\hat{\mathbf{r}}_{ij} \cdot \hat{\mathbf{u}}_i)(\hat{\mathbf{r}}_{ji} \cdot \hat{\mathbf{u}}_j)$	0	1	0	-1	1

Table 1. Any two configurations (columns) differ in at least one term.

Lipids in a lamellar bilayer mostly remain parallel or antiparallel to each other. Such a preference for alignment can be implemented in SiMPLISTIC simply by using a $|\hat{\mathbf{u}}_i \cdot \hat{\mathbf{u}}_j|^m$ factor in the expression for ε_{wd} . m is a non-negative, floating-point parameter that is included in order to regulate the strength of the aligning torque.

In view of all the above, and noting that we have already introduced an energy scale ε_0 while defining $V^{\text{Steric}}(r)$ in Eq. (6), let us now propose the following ansatz:

$$\varepsilon_{\text{wd}} = \varepsilon_0 (\hat{\mathbf{u}}_i \cdot \hat{\mathbf{u}}_j) |\hat{\mathbf{u}}_i \cdot \hat{\mathbf{u}}_j|^m \left[1 + a (\hat{\mathbf{r}}_{ij} \cdot \hat{\mathbf{u}}_i)(\hat{\mathbf{r}}_{ji} \cdot \hat{\mathbf{u}}_j) \right] \left[1 - b \frac{(\hat{\mathbf{r}}_{ij} \cdot \hat{\mathbf{u}}_i + \hat{\mathbf{r}}_{ji} \cdot \hat{\mathbf{u}}_j)}{2} \right]$$

This form of ε_{wd} is invariant under swapping of i and j but asymmetric under the inversion $\hat{\mathbf{u}}_i \rightarrow -\hat{\mathbf{u}}_i$, as desired (Sec. II.A.3). Also, ε_{wd} for the SSP and SSA configurations are respectively ε_0 and $-\varepsilon_0$, which complies with the sign criterion given in the first row of Eq. (4). Note that, of the three parameters— m , a and b , m has no effect on the values of ε_{wd} for the different canonical configurations because $|\hat{\mathbf{u}}_i \cdot \hat{\mathbf{u}}_j| = 1$ for each of them. We, therefore, need to tune a and b in order to make ε_{wd} satisfy the remaining conditions in Eq. (4). It may also be noted that, fixing a and b this way, leaves m as the only free parameter of the model well-depth, which is very much desirable as the number of parameters becomes minimal.

The two unknowns a and b can be solved for if ε_{wd} is known for any two of the collinear canonical configurations. To this aim, let us choose ε_{wd} for the configurations TTC and HTC simply as ε_0 and $-\varepsilon_0$ respectively, in compliance with the sign conditions in Eq. (4). Solving for a and b now, we get $a = 2$, $b = 4/3$. Table 2 lists the resulting values of ε_{wd} for all the canonical configurations. As can be readily verified using these values, for $kT_{\text{fluid}} \approx O(\varepsilon_0)$, all the

^f A spheroid is an ellipsoid of revolution and hence is uniaxial or axisymmetric. The GB spheroid is a computationally efficient approximation to an actual spheroid.

^g For a corresponding MC study, a spherocylindrical core should give the same results as what we obtained using the GB spheroid and MD.

^h Deserno et al.³⁰ used a computationally expensive trigonometric function for the tail. Our cubic spline was much cheaper but useful.

conditions given in Eq. (4) are satisfied.

SSP	TTC	SSA	HTC	HHC
ε_0	ε_0	$-\varepsilon_0$	$-\varepsilon_0$	$-7\varepsilon_0$

Table 2. Well-depth ε_{wd} for the canonical configurations in Figure 2.

C. Model Summary

To summarize, SiMPLISTIC represents lipids in implicit solvent as directed spheroids, which interact using the following potential.

$$V_{ij}(r) = 4\varepsilon_0 \left(\frac{1}{R^{12}} - \frac{1}{R^6} \right) + \varepsilon_0 - \varepsilon_{\text{wd}}, \text{ if } r < r_{\text{zf}}$$

$$= \varepsilon_{\text{wd}} \frac{(r_{\text{cut}} - r)^2 (3r_{\text{zf}} - 2r - r_{\text{cut}})}{\text{range}^3}, \text{ if } r_{\text{zf}} \leq r < r_{\text{cut}} = r_{\text{zf}} + \text{range}$$

$$= 0, \text{ otherwise}$$

where

$$R = (r - \sigma_{GB} + \sigma_0) / \sigma_0; r_{\text{zf}} = (2^{1/6} - 1)\sigma_0 + \sigma_{GB};$$

$$\varepsilon_{\text{wd}} = \varepsilon_0 (\hat{\mathbf{u}}_i \cdot \hat{\mathbf{u}}_j) |\hat{\mathbf{u}}_i \cdot \hat{\mathbf{u}}_j|^m \left[1 + 2(\hat{\mathbf{r}}_{ij} \cdot \hat{\mathbf{u}}_i)(\hat{\mathbf{r}}_{ji} \cdot \hat{\mathbf{u}}_j) \right] \left[1 - \frac{2}{3}(\hat{\mathbf{r}}_{ij} \cdot \hat{\mathbf{u}}_i + \hat{\mathbf{r}}_{ji} \cdot \hat{\mathbf{u}}_j) \right] \quad (8)$$

For the SSP and SSA configurations, $V_{ij}(r)$ is illustrated in Figure 4.

Apart from the lipid length σ_e , which only affects the spheroidal contact distance σ_{GB} [Eq. (5)], SiMPLISTIC has only two parameters, viz. *range* and *m*. The *range* parameter determines the number of interacting pairs of molecules and hence, quite trivially, affects the overall binding energy of the lipid aggregates which, in turn, affects thermal stability and elasticity^{30,31}. *m*, on the other hand, tunes the degree of alignment between the interacting lipids and therefore, for sufficiently large values, should guarantee the formation of bilayers where the lipids possess high orientational order. In the next section, we shall test this hypothesis and also examine SiMPLISTIC's self-assembly behavior for smaller values of *m*.

III. SELF-ASSEMBLY, TUNEABILITY, MIXING RULE

In this section we report self-assembly behavior of SiMPLISTIC (as seen in MD simulations for different values of *m*), analyze it and extend SiMPLISTIC to model new cases based on that analysis.

A. MD Study

1. Protocol

Self-assembly in an implicit solvent system is usually studied under the NVT ensemble for both MD^{26,31,48} and MC^{28,49} simulations. For our MD simulations, we chose the Nosé-Hoover thermostat⁵⁰, with separate temperature control variables coupled to the translational and rotational degrees of freedom for faster equilibration⁵¹. Thermostatted translational motion was integrated using the leap-frog scheme given in the Appendix of Ref. 52. For the rotational motion, the integrator described in Ref. 53 was used.

The system consisted of 1600 identical lipids in a cubic simulation box with periodic boundary conditions (PBC). To work in reduced units, each of the three constants— σ_0 , ε_0 , and the mass (μ) of each lipid, was taken as unity. The MD timestep was chosen to be $0.0035\sqrt{\mu\sigma_0^2/\varepsilon_0}$. Regarding the lipid length, we note that aspect ratios $\approx 1:3$ have been employed in several previous works on lipid modeling^{26,29,30,37}. In view of this, we also chose lipid length $\sigma_e = 3\sigma_0$. To make the rotational timescale comparable to the translational one, the moment of inertia (about the c.m) for each lipid was chosen to be $4\mu\sigma_0^2$.

Although *range* was featured as a free parameter of SiMPLISTIC in Sec. II.C, it is easy to see that a desired value of kT_{fluid} restricts the

choices for *range*. This is because too small a value of *range* would lead to insufficient binding in the face of thermal kinetic energy, and too large a value would turn the lipid aggregate into a tightly bound crystal or gel. For convenience, one might want $kT_{\text{fluid}} \approx \varepsilon_0$, and therefore we probed different values of *range* at $kT = \varepsilon_0$. *range* = σ_0 and $2\sigma_0$ did not show self-assembly, but *range* = $3\sigma_0$ did. Moreover, at this value of *range* the bilayer also remained fluid (this will be discussed later in the context of bilayer characteristics, in Sec. IV.A). Later we found that *range* = $2.5\sigma_0$ also gives stable phases at $kT = \varepsilon_0$. We, however, performed simulations mostly with *range* = $3\sigma_0$ because it leads to faster self-assembly and gives the hydration force a range comparable to the lipid length.

In order to study spontaneous, free self-assembly from a disordered, isotropic phase under NVT, choosing an appropriate number density is very important. Implicit solvent systems are far less dense than anhydrous systems such as systems of mesogens, simply because there is an implicit presence of water in the form of unoccupied volume within the simulation box. Too low a number density, however, is not conducive to self-assembly as can be verified easily. One way to get a viable number density for ISCG lipid systems is to start with an approximately valid preassembled structure such as a system of well-separated bilayers. The disordered, isotropic configuration can then be generated simply by evaporating the preassembled structure at a high temperature under NVT. This way of producing a randomized initialization also eliminates any undesirable core-core overlap between the lipids²⁸. As depicted in Figure 5, we generated our disordered, isotropic configuration by evaporating two lattice membranes that were assembled on square grids. To ensure enough space in the simulation box, the two bilayers were kept out of each other's range of interaction, viz. the interbilayer separation was made greater than *range*. This resulted in a box size of $21.3\sigma_0$ and number density of $0.166\sigma_0^{-3}$. All lipids in the disordered phase were then allocated random velocities from the Maxwell-Boltzmann distribution at $kT = \varepsilon_0$ and self-assembly was studied for that temperature for different values of *m*. We infer that the lipids were free to arrange themselves during self-assembly because the overall internal pressure or stress, as computed using the virial⁵⁴, remained near zero.

2. Self-assembly

Self-assembly was studied for $m = 0, 0.5, 1, \dots, 4$ at $kT = \varepsilon_0$. Figure 6 shows some of the phases obtained. Self-assembly was rapid with structure being discernible by 4000 steps and prominent aggregate formation by 6000 steps. For $0 \leq m \leq 3$, closely packed inverted micelles were obtained, with the micellar curvature decreasing with increasing *m*. For $m > 3$, a preference for bilayer formation was clearly visible, with almost no negatively curved phase remaining in the simulation box at $m = 4$. The parameter, *m*, therefore, determines whether the self-assembled phase will be non-lamellar or lamellar. We also studied self-assembly for some random values of $m > 4$ and only lamellar bilayers were obtained. To summarize our observations, the maximal curvature for non-lamellar phase is obtained for $m = 0$, the curvature of non-lamellar phase decreases with increasing *m*, and no intrinsic curvature, negative or positive, remains in the system for $m \geq 4$.

B. How *m* tunes curvature

To explain the aforementioned observations, let us analyze how *m* affects the energy of lipid splay. We define splay as any configuration between a pair of lipids *i* and *j* where each lipid is a mirror image of the other with respect to a mirror plane that bisects and is normal to \mathbf{r}_{ij} . The angle between the lipids is called the splay angle, θ (Figure 7). Note that $\theta = 0, \pi, -\pi$ lead to the SSP, TTC and HHC configurations respectively (cf. Figure 2). As seen from the plot in Figure 7, the most

preferred splay angle θ_{\max} , viz. θ at which ε_{wd} is maximum, is negative for each $m \geq 0$. Also, the amount of splay in this configuration, viz. $|\theta_{\max}|$, decreases with increasing m . Notice that, because the model lipids are cylindrically symmetric, a preference for non-zero splay implies a conical molecular profile. If the most preferred splay angle is negative, viz. $\theta_{\max} < 0$, the effective molecular shape must be that of an inverted cone with the angle between the cone axis and cone surface given by $|\theta_{\max}|/2$. Inverted cones form non-lamellar phases with negative intrinsic curvatures such as the inverted micelles. As $\theta_{\max} \rightarrow 0$, the effective molecular shape becomes cylindrical which favors the formation of lamellar bilayers with zero spontaneous curvature. From this perspective, it is clear how θ_{\max} governs the spontaneous curvature of the self-assembled phases. Because θ_{\max} , in turn, is tuned by m as discussed above (Figure 7), this explains the observations reported in Sec. III.A.2. Note that this also shows how, despite having a fixed spheroidal core, SiMPLISTIC lipids can have their effective shape or packing parameter⁵⁵ varied with m and thus exhibit polymorphism on self-assembly.

C. Mixing Rule for Lipids with Different Values of m

A logical extension of the discussion in the last subsection (Sec. III.B) is to ask how to model the interaction between a pair of SiMPLISTIC lipids each of which generates a different spontaneous curvature in single-component self-assembly. In other words, we seek to extend SiMPLISTIC so that mixtures of lipids with different packing parameters, such as lamellar and non-lamellar lipids, can be simulated.

To this end, let us take two types of SiMPLISTIC lipids, A and B, which differ only in the parameter m . From the geometry of cones it follows, $\theta_{\max}^{\text{AB}} = (\theta_{\max}^{\text{AA}} + \theta_{\max}^{\text{BB}})/2$. This implies that m for the A-B interaction must be intermediate between that for the A-A and B-B interactions. In keeping with this and the widely adopted Lorentz-Berthelot mixing rule, we propose $\varepsilon_{\text{wd}}^{\text{AB}} = \sqrt{\varepsilon_{\text{wd}}^{\text{AA}} \cdot \varepsilon_{\text{wd}}^{\text{BB}}}$, which gives

$$m_{\text{AB}} = \frac{m_{\text{AA}} + m_{\text{BB}}}{2}. \quad (9)$$

A two-component mixture of A and B lipids can now be studied with the interactions A-A, B-B and A-B each following Eq. (8) with $m = m_{\text{AA}}$, m_{BB} and m_{AB} respectively. To test the validity of this mixing rule, we studied self-assembly for a binary mixture of 800 lamellar and 800 non-lamellar lipids with $m = 4$ and 0 respectively. Figure 8 depicts a few close-ups of the aggregates formed. Note how the lamellar lipids (shown in red) intermix with the non-lamellar lipids (shown in green) in forming the inverted micelle (Figure 8c). The preference of the lamellar lipids to form bilayers is also discernible from the lamellar clusters of the red lipids just beside the inverted micelle (Figure 8b).

IV. MODEL MEMBRANES, HYDROPHOBIC MISMATCH

This section reports how SiMPLISTIC performs for model membrane simulations. Later in this section, we shall also discuss an extension of SiMPLISTIC to include the effect of hydrophobic mismatch in multicomponent bilayers. Because SiMPLISTIC is required to model only lamellar lipids for membrane simulations, we must take $m \geq 4$ in view of the self-assembly results reported in Sec. III.A.2. All simulations, however, are performed with $m = 4$ only (also see Sec. IV.A.4 for further remarks).

A. Bilayer Characteristics

Model membrane simulations are usually performed under zero lateral tension^{30,32}. For such constant tension simulations, we adopted a two-dimensional Nosé-Hoover NPT dynamics⁵⁴ in the bilayer plane to regulate the lateral pressure. To prepare the initial state, a preassembled

box-spanning bilayer was thermalized at $kT = \varepsilon_0$ under zero tension. As desired, the surface tension, measured using the diagonal elements of the internal pressure tensor⁵⁶, remained near zero⁵⁷ for every production run.

1. Lateral diffusivity, area per lipid : Fluid and gel phases

The in-plane or lateral diffusivity (D_{\parallel}) of lipids in the membrane is computed from the limiting slope of the mean square displacement (MSD) in the bilayer plane, using the Einstein relation for two-dimensional diffusion^{58,59}. Figure 9 depicts the MSDs plotted for four NVE runs starting with equilibrated tensionless bilayers, with different mean temperatures. The corresponding diffusivities and projected area per lipid (A_L) are listed in Table 3.

kT	0.46	0.74	0.94	1.11
D_{\parallel}	1.11×10^{-2}	2.60×10^{-2}	9.94×10^{-2}	0.348
A_L	0.99	1.04	1.16	1.30

Table 3. Lateral diffusivity (D_{\parallel}) and area per lipid (A_L) at various temperatures (kT). Units: D_{\parallel} in $\sigma_0 \sqrt{\varepsilon_0/\mu}$, A_L in σ_0^2 , kT in ε_0 .

A fluid-gel transition is typically associated with significant drop in D_{\parallel} , reduction of A_L and increased (hexagonal) bond orientation order²⁸. From the MSDs plotted in Figure 9 and a visual inspection of the lipid arrangement in the bilayers depicted there, it is apparent that the membrane is fluid at $kT = 1.1\varepsilon_0$ and $0.94\varepsilon_0$ and gel at $kT \leq 0.74\varepsilon_0$. Our objective of generating a fluid phase at $kT_{\text{fluid}} \approx \varepsilon_0$ (Sec. III.A.1) is therefore fulfilled.

2. Order parameter

The orientational (uniaxial) order parameter for lipids in a bilayer is given as $\frac{1}{2} \langle 3(\hat{\mathbf{u}}_i \cdot \hat{\mathbf{n}})^2 - 1 \rangle_i$, where $\hat{\mathbf{n}}$ is a unit vector along the average normal of the bilayer. For a tensionless membrane at kT_{fluid} , the order parameter of SiMPLISTIC lipids is 0.967. From this high amount of orientational order, and a visual inspection of the side view of the bilayer as provided in Figure 9, it is safe to infer that the fluid bilayer is not tilted. No tilt was found in the gel phase as well.

3. Bilayer thickness

The thickness of a bilayer is estimated as follows. Taking the X and Y axes in the bilayer plane, the bilayer thickness lies along the Z direction. The Z coordinate of the head end of a lipid is given by

$$h_{\text{h}} = \left(\mathbf{r} + \frac{\sigma_{\text{c}}}{2} \hat{\mathbf{u}} \right) \cdot \hat{\mathbf{n}}.$$

The bilayer thickness may be estimated as the spread in the distribution of h_{h} , which is computed as twice the standard deviation of h_{h} . For a tensionless fluid membrane, we found the thickness to be $6.297\sigma_0$. In contrast, for a crystalline flat bilayer with no tilt or interdigitation, the thickness must be $2\sigma_{\text{c}} = 6\sigma_0$. Because our fluid membrane is thicker than this, it implies that there is no interdigitation in the fluid phase, as is also apparent from the side view of the bilayer in Figure 9. No interdigitation was found in the gel phase as well.

4. Bending modulus

Being designed with a top-down, phenomenological approach, getting the membrane elasticity such as the bending rigidity right is a decisive factor for SiMPLISTIC. All other top-down attempts at ISCG modeling of lipids with rigid models^{25–28} had failed to produce experimentally relevant values for the bending moduli, as was mentioned in Sec. I. There are several methods for determining the bending modulus κ_{c} from configurations generated by molecular simulations⁶⁰. Of these, a method based on spectral analysis of the

height fluctuations of a tensionless bilayer has been used by most previous works on ISCG modeling of lipids. This method is difficult and computationally expensive, which has to do with its requirement of very large system sizes (continuum limit)³¹ and a robust sampling of global bilayer undulations to apply the Fourier transform on. In contrast, a relatively recent and computationally simpler method⁶¹ based on real-space fluctuations (RSF) of the splay degrees of freedom is local in nature and, therefore, can be applied to rather small system sizes (as small as ~ 100 lipids), which makes it more practical for MD simulations. This method has also been successfully validated on a range of lipid systems⁶². For our case of flat bilayer composed of SiMPLISTIC lipids with director $\hat{\mathbf{u}}$, the RSF method is briefly described as follows.

According to the RSF methodology^{61,63} the splay at any point \mathbf{p} on the bilayer is given as the local covariant derivative of the vector field $\hat{\mathbf{u}} - \hat{\mathbf{n}}$ along any vector $\hat{\mathbf{e}}_\alpha$ tangent to the bilayer. Because the bilayer normal $\hat{\mathbf{n}}$ does not vary across a flat bilayer and $\hat{\mathbf{n}} \cdot \hat{\mathbf{e}}_\alpha = 0$, the splay is given as

$$S_\alpha = \lim_{\Delta \rightarrow 0} \frac{[\hat{\mathbf{u}}(\mathbf{p}) - \hat{\mathbf{u}}(\mathbf{p} + \Delta \hat{\mathbf{e}}_\alpha)] \cdot \hat{\mathbf{e}}_\alpha}{\Delta}. \quad (10)$$

Computationally, S_α may be approximated as $\left[(\hat{\mathbf{u}}_i - \hat{\mathbf{u}}_j) \cdot \hat{\mathbf{e}}_\alpha \right] / (\mathbf{r}_{ij} \cdot \hat{\mathbf{e}}_\alpha)$ where $\{i, j\}$ is a pair of nearest neighbor lipids from the same leaflet. The bilayer bending rigidity κ_C is related to the frequency distribution of S_α as

$$f(S_\alpha) \propto \exp\left(-\frac{\kappa_C S_\alpha^2 A_\perp}{2kT}\right). \quad (11)$$

κ_C/kT can therefore be determined from the variance of a Gaussian with zero mean fitted to the frequency distribution of S_α (Figure 10). Employing this method, we computed the bending rigidity of a tensionless SiMPLISTIC bilayer at five different temperatures, as listed in Table 4.

Phase	Fluid			Gel	
kT	1.20	1.11	1.00	0.80	0.46
κ_C/kT	24.6	28.3	36.9	56.5	106.9
κ_C	29.5	31.4	36.9	45.2	49.2

Table 4. Bending modulus (κ_C) at various temperatures (kT). Both κ_C and kT are in units of ϵ_0 .

κ_C/kT of fluid biological membranes without cholesterol falls within the range 5–30.^{64,65} Our numerical estimates for fluid SiMPLISTIC bilayers also fall within this range for $kT \geq 1.11\epsilon_0$ (Table 4). With $kT_{\text{fluid}} = 1.11\epsilon_0$ or more, SiMPLISTIC therefore successfully reproduces experimentally relevant values for the bending stiffness. This also proves that a rigid, molecular level model of lipids, if designed properly, is capable of generating valid bending moduli for model membranes, despite being stiffer than the flexible bead-spring models (such as Ref. 29,30,49) that have so far provided the only means to this end.

Remarks on our choice of m : As mentioned before, all model membrane simulations were performed with $m = 4$. Why choose only $m = 4$ when $m > 4$ also give lamellar bilayers (Sec. III.A.2)? As shown in Figure 7, increase in m leads to a preference for decreased amount of splay. Because bending stiffness is inversely proportional to the variance of the splay distribution [Eq. (11)], this implies that κ_C increases with m . With $m = 4$, κ_C/kT already lies near the upper end

of the experimentally interesting range (Table 4). $m > m_{\text{max}}$ for some $m_{\text{max}} \geq 4$ would therefore lead to unrealistically large values for κ_C/kT that lie outside this range. Hence, most values of $m > 4$ are not relevant. One may, however, still probe how big m can get, viz. m_{max} , without generating too big a bending modulus. We leave this exercise for future works.

5. Area compressibility modulus and elastic ratio

For constant tension simulations where the membrane area fluctuates about a mean value to regulate the surface tension, the best suited measure for area compressibility modulus κ_A is given by⁵⁶

$$\kappa_A = \frac{kT \langle A \rangle}{\langle A^2 \rangle - \langle A \rangle^2} \quad (12)$$

where A denotes the total (projected) area of the membrane and $\langle \rangle$ denotes the time average obtained from a production run of the simulation. The elastic ratio is a dimensionless quantity defined as

$$b = \kappa_A h^2 / \kappa_C = \frac{\langle A \rangle h^2}{\langle A^2 \rangle - \langle A \rangle^2} \left/ \left(\frac{\kappa_C}{kT} \right) \right. \quad (13)$$

where h denotes the membrane thickness^{28,29}. b ranges from 4–12 for bilayers with strong interleaflet coupling and 16–48 for unconnected bilayers⁶⁶. The upper limit $b = 48$ is for bilayers where the two leaflets can freely slide past each other^{65,67}. Experimental systems give b in the range 20–30.⁶⁵ At least two explicit solvent simulations gave $b = 48$.^{67,68} Our estimates for well-equilibrated SiMPLISTIC bilayers gave $b = 31.7$ at $kT = 1.20\epsilon_0$ and $b = 45.5$ at $kT = \epsilon_0$. These values indicate that there is no significant interleaflet coupling for SiMPLISTIC bilayers. This is expected because we eliminated a key source for such coupling⁶⁹, viz. lipid interdigitation between the opposing leaflets, by design (Sec. II.A.4 and IV.A.3).

B. Hydrophobic Mismatch

Hydrophobic mismatch is a key player in the physics of multicomponent lipid membranes if the constituent lipids differ in length due to a difference in either chain length or chain saturation^{70–72}. Such difference in length between neighboring lipids in a leaflet exposes some of the hydrophobic parts of the longer lipid(s) to the surrounding water, which is unfavorable. To avoid this ‘hydrophobic mismatch’, lipids prefer to be surrounded by lipids with similar length, which may lead to a demixing of dissimilar lipids in the multicomponent system⁷³. In other words, hydrophobic mismatch generates a line tension that, if large enough, may generate phase separation through domain formation^{72,74,75}.

SiMPLISTIC, as defined so far (Sec. II.C and III.C), can only model systems where all lipids have the same length (σ_e in Sec. II.B.1). In order to model multicomponent membranes with hydrophobic mismatch, it therefore needs to handle interactions between lipids with different lengths. We extend SiMPLISTIC in the following by defining just such an interaction and test our model with simulations.

Let us take two types of SiMPLISTIC lipids (A and B) that differ only in their spheroidal lengths, σ_e^A and σ_e^B . The contact distance between two such GB spheroids of unequal lengths had been worked out by Cleaver et al.⁷⁶. Accordingly, the contact distance $\sigma(\hat{\mathbf{r}}_{ij}, \hat{\mathbf{u}}_i, \hat{\mathbf{u}}_j)$ between a lipid i of type A and another lipid j of type B is given as

$$\sigma = \sigma_0 \left[1 - \left\{ \frac{\chi_A (\hat{\mathbf{r}}_{ij} \cdot \hat{\mathbf{u}}_i)^2 + \chi_B (\hat{\mathbf{r}}_{ji} \cdot \hat{\mathbf{u}}_j)^2 + 2\chi_A \chi_B (\hat{\mathbf{r}}_{ij} \cdot \hat{\mathbf{u}}_i)(\hat{\mathbf{r}}_{ji} \cdot \hat{\mathbf{u}}_j)(\hat{\mathbf{u}}_i \cdot \hat{\mathbf{u}}_j)}{1 - \chi_A \chi_B (\hat{\mathbf{u}}_i \cdot \hat{\mathbf{u}}_j)^2} \right\} \right]^{-1/2} \quad (14)$$

where χ_A and χ_B denote the anisotropy parameters of i and j respectively, as defined in Sec. II.B.1. Note that for i and j lipids having identical lengths, $\chi_A = \chi_B = \chi$, which reduces σ in Eq. (14) to σ_{GB} in Eq. (5). With the contact distance (σ) obtained as above, we can now choose Eq. (6) as the steric part of the potential between i and j , with R now defined as $R = (r - \sigma + \sigma_0) / \sigma_0$.

Hydrophobic mismatch driven demixing, interpreted as a tendency of lipids of similar length to cluster together within a leaflet, can be modeled through the mechanism of like lipids interacting more strongly than unlike ones. This is most easily achieved by simply reducing the strength of A-B interaction compared to that of A-A and B-B. Care must however be taken to do this for lipids within the same leaflet only. Otherwise, the weaker attraction between unlike lipids from opposing leaflets would lead to direct interleaflet coupling through domain registration. This is unphysical because hydrophobic mismatch, in reality, destabilizes registration rather than favoring it. For further illustration of this last point the reader is referred to Ref. 74 and the Fig. 2 and its corresponding discussion in Ref. 77.

In view of the above, let us define the energy scale (viz. ε_0 as defined in Sec. II.B) for the different pair interactions as

$$\begin{aligned} \varepsilon_0^{AA} &= \varepsilon_0^{BB} = \varepsilon_0 \\ \varepsilon_0^{AB} &= [1 - p(\sigma_e^A, \sigma_e^B)] \varepsilon_0 \\ \text{where} & \\ p(\sigma_e^A, \sigma_e^B) &> 0, \text{ for } \sigma_e^A \neq \sigma_e^B \text{ within same leaflet} \\ &= 0, \text{ otherwise} \end{aligned} \quad (15)$$

We, therefore, need to define $p(\sigma_e^A, \sigma_e^B)$ now. To this end, note that this p can be interpreted as a dimensionless penalty factor which determines the loss of binding energy due to lipid length mismatch. This loss of binding energy is what gives rise to a line tension λ between two domains of unlike lipids within a leaflet, and is directly proportional to it⁷². The line tension between domains of A and B, therefore, is directly proportional to the penalty factor, i.e. $\lambda \propto p$. Kuzmin et al.⁷⁸, in Eq. 17 of their paper, have derived a quadratic dependence of the line tension on (δ/h_0) , where δ is the amount of hydrophobic mismatch and h_0 is the average thickness of the stretches of leaflet within the two domains. This dependence is exact if the two domains have the same spontaneous curvature, which is a condition that applies well for flat membranes composed of lamellar lipids. In our case, $\delta = |\sigma_e^A - \sigma_e^B|$ and $h_0 = (\sigma_e^A + \sigma_e^B)/2$. Because p scales with λ and λ scales with $(\delta/h_0)^2$ as discussed above, we may define p as

$$p(\sigma_e^A, \sigma_e^B) = \nu (\sigma_e^A - \sigma_e^B)^2 / \left(\frac{\sigma_e^A + \sigma_e^B}{2} \right)^2 \quad (16)$$

where ν is a positive, floating-point parameter that can be used to tune the line tension.

The interaction potential for a pair of A and B lipids is therefore given by Eq. (8) with the replacements $\sigma_{GB} \rightarrow \sigma$ and $\varepsilon_0 \rightarrow \varepsilon_0^{AB}$ where σ and ε_0^{AB} are given by Eq.s (14) and (15) respectively. Note that with each lipid residing in either of the two leaflets of a flat membrane, the directed axes (viz. $\hat{\mathbf{u}}$) of a pair of lipids form an acute angle if the lipids are in the same leaflet and obtuse angle otherwise. Therefore, the

condition for a pair of A and B lipids being in the same leaflet, and hence interacting with reduced strength, is simply $\hat{\mathbf{u}}_A \cdot \hat{\mathbf{u}}_B > 0$.

To test this model out, we simulated two-component membranes consisting of A and B lipids with $\sigma_e^A = 3\sigma_0$ and $\sigma_e^B = 4\sigma_0$, at $kT = \varepsilon_0$ and vanishing surface tension, for different values of ν . Starting from a randomly mixed state, no demixing was apparent for $\nu = 1, 2$ even after long runs $\sim 10^5$ MD steps. This suggests that the corresponding line tensions for these smaller values of ν are not large enough to outweigh the entropic preference towards well-mixed states at $kT = \varepsilon_0$. With the increased line tension for $\nu \geq 3$, however, clusters of like lipids appeared with excellent large scale domain formation at $\nu = 5$ (Figure 11). As desired, no domain registration was observed between the opposing leaflets of the bilayer (Figure 11). SiMPLISTIC therefore, with the inclusion of interaction between lipids of different lengths as described above, succeeds in modeling hydrophobic mismatch.

V. CONCLUSION

A. Highlights

This paper described a novel, coarse-grained model called ‘SiMPLISTIC’ for large scale, particle based simulations of lamellar and non-lamellar lipid systems in implicit water. In absence of explicit water, the hydrophobic effect and the hydration force are mimicked with lipid-lipid attraction and repulsion respectively. SiMPLISTIC abbreviates for ‘Single-site Model with Pairwise Interaction for Lipids in Implicit Solvent with Tuneable Intrinsic Curvature’. The most important features of SiMPLISTIC are listed below.

- SiMPLISTIC lipids are single-site and rigid. The soft-core, anisotropic, pair potential (Sec. II.C) contains only three parameters that relate to the following— the lipid length (σ_e), the interaction range (*range*) and the packing parameter (m).
- SiMPLISTIC is a phenomenological model (Sec. II.A.4) designed for speed (Sec. V.B) and simplicity (Sec. II.A.3). The anisotropic nature of the SiMPLISTIC potential gives it a unique ability to model the hydration force between lipid aggregates as soft repulsions for certain relative orientations.
- The model lipids show rapid, unassisted self-assembly (Sec. III.A.2). The free parameter m determines the curvature of the self-assembled phase (Sec. III.B). Smaller values of m generate inverted micelles and larger values, bilayers.
- SiMPLISTIC includes mixing rules (Sec. III.C) for modeling mixtures of lipids with different packing parameters.
- Model membrane simulations with bilayer forming SiMPLISTIC lipids show fluid-gel transition (Sec. IV.A.1) and yield experimentally relevant values for the bending stiffness in the fluid phase (Sec. IV.A.4). The bilayers are tilt-free (Sec. IV.A.2) and do not show interdigitation (IV.A.3). SiMPLISTIC membranes also give satisfactory elastic ratios (derived from the area compressibility modulus) that suggest the two leaflets of a SiMPLISTIC bilayer are not coupled strongly (Sec. IV.A.5).
- A simple extension of SiMPLISTIC to model hydrophobic mismatch (Sec. IV.B) successfully generates demixing through phase separation in two-component model membranes.

B. Benchmarks

SiMPLISTIC is designed for speed. Here we report some crude benchmarks for SiMPLISTIC and compare it with some other relevant models.

The execution time of an optimized code is not a very meaningful metric for the underlying model’s computational efficiency. This is because, apart from the platform, CPU time depends on the

optimizations performed within the source code as well as during compilation, both of which are subject to variation from one implementation to another. Benchmarks under non-optimal conditions, on the other hand, are more useful because they represent the least performance expected from a model running on any given processor. With this in mind, we benchmarked SiMPLISTIC as follows.

The test code, implemented in Fortran 90 with double precision for the floating-points, consisted of just the SiMPLISTIC force routines and the Nosé-Hoover NVT integrator. To eliminate I/O calls during run, no configuration dumping was done. No parallelization or SIMD vectorization and no domain decomposition or neighbor list were applied – hence, the force routines enumerated every possible pair of lipids serially in the least efficient way. The compilation was done using gfortran with no optimization. The simulated system was the same as reported in Sec. III.A.1, with $m=1$ and starting from a self-assembled phase of closely packed inverted micelles at $kT = \varepsilon_0$.

Although the code ran serially on a single core, no core affinity or task priority was set. Running this test code for several times on a laptop with an Intel i3 processor (clock speed 2.13 GHz) and 32-bit GNU/Linux, we consistently obtained CPU times of 2.05 minutes per 1000 MD steps. We also timed the self-assembly of the same system at 6.06 minutes (6000 MD steps). It goes without saying that with multicore parallelization, SIMD vectorization and GPU accelerations that are routinely performed nowadays, the execution time will be improved manifold. It may also be pointed out that the computation of $|\hat{\mathbf{u}}_i \cdot \hat{\mathbf{u}}_j|^m$ [Sec. II.B.3 and Eq. (8)] for floating point m has a significant overhead in SiMPLISTIC. This is because such floating-point powers are computed using logarithms followed by exponentials – both of which operations are quite expensive. For integer m , however, $|\hat{\mathbf{u}}_i \cdot \hat{\mathbf{u}}_j|^m$ may be computed much faster because odd and even powers are best computed using a few (recursive) multiplications only.

To compare the computational performance of SiMPLISTIC to that of a standard single-site, rigid model with a similar anisotropic pair potential (viz. Gay-Berne⁴⁰), and also a multi-site, bead-spring model for lipids in implicit solvent (viz. the Cooke-Kremer-Deserno model³⁰), consider the following. SiMPLISTIC contains less floating point operations (flops) than a switched Gay-Berne (GB) potential and therefore, should be faster than the GB benchmarks on any given platform. SiMPLISTIC is also faster than a single-site amphiphile model previously published by us³⁵, again by virtue of requiring fewer flops. Being single-site, this amphiphile model was found to be more than 1.6 times faster than a rigid version of the multi-site Cooke-Kremer-Deserno model, which, in turn, is naturally faster than the original flexible (bead-spring) version³⁰. SiMPLISTIC, therefore, should be more efficient than the Cooke-Kremer-Deserno model for large scale phenomena that are not significantly sensitive to lipid chain flexibility.

C. Scope

In view of the features listed in Sec. V.A, SiMPLISTIC should be able to serve as an excellent model for large-scale lipid simulations in academic and industrial research. Apart from research, the model should also be effective in education. For example, SiMPLISTIC's conceptual simplicity, versatility and computational speed make it an ideal model for learning about complex, cooperative phenomena in lipid-based systems through hands-on, interactive simulations.

To inspire future applications, some specific use cases for SiMPLISTIC are suggested below.

- Studying the discontinuous cubic phase (Fd3m) formed by inverted micelles.
- Studying elasticity and nanoscale dynamics in multicomponent membranes as functions of the membrane constitution.
- Studying vesicles consisting of lamellar lipids on the outer

surface and non-lamellar lipids on the inner. Hydrophobic mismatch driven demixing may induce budding in multicomponent vesicles.

- Modeling cholesterol as a non-lamellar lipid present in membranes composed of lamellar lipids. This, linked with SiMPLISTIC's ability to model hydrophobic mismatch and form lipid domains, might make studies of lipid rafts (or L_d - L_o phase separation) relevant.
- Studying tension induced membrane rupture or pore formation.
- Modeling symmetric (asymmetric) bolalipids as dimers composed of two SiMPLISTIC lipids with identical (different) m , in the spirit of Ref. 36.
- Modeling lipid nanoparticles, liposomes and cubosomes for therapeutic applications such as drug and gene delivery.
- Studying membrane permeability by probing the permeation of simple, sterically interacting, Brownian particles through SiMPLISTIC membranes.
- Interactive molecular dynamics.

D. Future Directions

1. Two more phases with negative curvature

Although the free parameter m tunes the spontaneous curvature continuously from inverted micelles to planar bilayers, it is curious that no inverted hexagonal (H_{II}) or bicontinuous/bilayer cubic (Q_{II}^B) phase was obtained through self-assembly in our simulations. We suspect that a cubic simulation box with periodic boundary conditions, as employed by us, cannot form the H_{II} phase due to the lack of hexagonal symmetry. On the other hand, because it involves curved bilayers, the Q_{II}^B phase would probably require a much larger system size. We hope to address these issues in future work(s).

2. Possible extensions of SiMPLISTIC

SiMPLISTIC, as defined in this paper, is useful for simulating systems consisting of uncharged lipids only. Extending SiMPLISTIC to include interactions with purely hydrophilic and hydrophobic particles, which may be in the form of GB spheroids or spheres, will significantly increase its scope. Such an extension, for example, might be useful in modeling lipid-protein interactions and studying membrane permeability or leakage of cargo from cubosomes and liposomes.

In addition to this, defining electrostatic charges on SiMPLISTIC lipids and other particles will make the model even more effective. Such an extension might enable probing important large scale phenomena such as lipid-DNA complex formation in the presence of counter-ions, fusion of oppositely charged vesicles etc.

3. An open question

SiMPLISTIC may be seen as a proof of concept, which demonstrates that a single-site, rigid model designed using some simple guidelines (Sec. II.A) can spontaneously self-assemble into fluid phases and generate elastic properties consistent with experiments and other simulations. Moreover, it shows how the intrinsic curvature of the self-assembled phase (or equivalently, the molecular packing parameter⁵⁵) may be tuned with only a single parameter. Our previous single-site and rigid amphiphile model³⁵ was also capable of tuning the curvature with a single parameter. However, that model gave phases with positive curvatures, whereas SiMPLISTIC gives phases with negative curvatures. To resolve this dichotomy, it is natural to imagine a single-site, rigid model that can self assemble into phases with all possible curvatures– both positive and negative. Apart from its sheer elegance, such a minimalistic, molecular level model will also be extremely useful, as amphiphiles with any packing parameter may be modeled with it, including mixtures of molecules with different

effective shapes (packing parameters). Whether such an all-encompassing yet simple model can be designed is, however, an open question.

ACKNOWLEDGMENTS

Somajit Dey is funded by the Council of Scientific & Industrial Research (CSIR), India, through a Senior Research Fellowship [Grant No. 09/028(0960)/2015-EMR-I]. Dey thanks Dr. Sayantani Das for improving some of the illustrative figures.

AUTHOR INFORMATION

Somajit Dey — Email: sdphys_rs@caluniv.ac.in; Current Address: Department of Physics, University of Calcutta, 92, A.P.C. Road, Kolkata-700009, India; <https://orcid.org/0000-0002-6102-9777>

Jayashree Saha — Email: jsphy@caluniv.ac.in; Current Address: Department of Physics, University of Calcutta, 92, A.P.C. Road, Kolkata-700009, India;

REFERENCES

- (1) Mouritsen, O. G.; Bagatolli, L. A. *LIFE- AS A MATTER OF FAT Lipids in a Membrane Biophysics Perspective*; The Frontiers Collection; Springer International Publishing: Cham, 2016. <https://doi.org/10.1007/978-3-319-22614-9>.
- (2) Israelachvili, J. N.; Mitchell, D. J.; Ninham, B. W. Theory of Self-Assembly of Hydrocarbon Amphiphiles into Micelles and Bilayers. *J. Chem. Soc. Faraday Trans. 2 Mol. Chem. Phys.* **1976**, 72, 1525–1568. <https://doi.org/10.1039/F29767201525>.
- (3) Lombardo, D.; Kiselev, M. A.; Magazù, S.; Calandra, P. Amphiphiles Self-Assembly: Basic Concepts and Future Perspectives of Supramolecular Approaches. *Adv. Condens. Matter Phys.* **2015**, 2015. <https://doi.org/10.1155/2015/151683>.
- (4) Luzzati, V.; Delacroix, H.; Gulik, A.; Gulik-Krzywicki, T.; Mariani, P.; Vargas, R. The Cubic Phases of Lipids. *Stud. Surf. Sci. Catal.* **2004**, 148 (C), 17–40. [https://doi.org/10.1016/S0167-2991\(04\)80191-5](https://doi.org/10.1016/S0167-2991(04)80191-5).
- (5) Henriksen, J. R.; Andresen, T. L.; Feldborg, L. N.; Duelund, L.; Ipsen, J. H. Understanding Detergent Effects on Lipid Membranes: A Model Study of Lysolipids. *Biophys. J.* **2010**, 98 (10), 2199–2205. <https://doi.org/10.1016/j.bpj.2010.01.037>.
- (6) Helfrich, W. Lyotropic Lamellar Phases. *J. Phys. Condens. Matter* **1994**, 6 (23A). <https://doi.org/10.1088/0953-8984/6/23A/009>.
- (7) Damodaran, K. V.; Merz, K. M. Computer Simulation of Lipid Systems. In *Reviews in Computational Chemistry V*; Lipkowitz, K. B., Boyd, D. B., Eds.; VCH Publishers, Inc, 2007; pp 269–298. <https://doi.org/10.1002/9780470125823.ch5>.
- (8) Tenchov, B.; Koynova, R. Cubic Phases in Membrane Lipids. *Eur. Biophys. J.* **2012**, 41 (10), 841–850. <https://doi.org/10.1007/s00249-012-0819-3>.
- (9) Van Meer, G.; De Kroon, A. I. P. M. Lipid Map of the Mammalian Cell. *J. Cell Sci.* **2011**, 124 (1), 5–8. <https://doi.org/10.1242/jcs.071233>.
- (10) van Meer, G.; Voelker, D. R.; Feigenson, G. W. Membrane Lipids: Where They Are and How They Behave. *Nat. Rev. Mol. Cell Biol.* **2008**, 9 (2), 112–124. <https://doi.org/10.1038/nrm2330>.
- (11) Basu Ball, W.; Neff, J. K.; Gohil, V. M. The Role of Nonbilayer Phospholipids in Mitochondrial Structure and Function. *FEBS Lett.* **2018**, 592 (8), 1273–1290. <https://doi.org/10.1002/1873-3468.12887>.
- (12) Azmi, I. D. M.; Moghimi, S. M.; Yaghmur, A. Cubosomes and Hexosomes as Versatile Platforms for Drug Delivery. *Ther. Deliv.* **2015**, 6 (12), 1347–1364. <https://doi.org/10.4155/tde.15.81>.
- (13) Koynova, R.; Tenchov, B.; Macdonald, R. C. Nonlamellar Phases in Cationic Phospholipids, Relevance to Drug and Gene Delivery. *ACS Biomater. Sci. Eng.* **2015**, 1 (3), 130–138. <https://doi.org/10.1021/ab500142w>.
- (14) Kulkarni, C. V. Lipid Self-Assemblies and Nanostructured Emulsions for Cosmetic Formulations. *Cosmetics* **2016**, 3 (4). <https://doi.org/10.3390/cosmetics3040037>.
- (15) Akbarzadeh, A.; Rezaei-Sadabady, R.; Davaran, S.; Joo, S. W.; Zarghami, N.; Hanifehpour, Y.; Samiei, M.; Kouhi, M.; Nejati-Koshki, K. Liposome: Classification, Preparation, and Applications. *Nanoscale Res. Lett.* **2013**, 8 (1), 1. <https://doi.org/10.1186/1556-276X-8-102>.
- (16) Eeman, M.; Deleu, M. From Biological Membranes to Biomimetic Model Membranes. *Biotechnol. Agron. Soc. Environ.* **2010**, 14 (4), 719–736.
- (17) Daraee, H.; Etemadi, A.; Kouhi, M.; Alimirzalu, S.; Akbarzadeh, A. Application of Liposomes in Medicine and Drug Delivery. *Artif. Cells, Nanomedicine Biotechnol.* **2016**, 44 (1), 381–391. <https://doi.org/10.3109/21691401.2014.953633>.
- (18) Balazs, D. A.; Godbey, W. Liposomes for Use in Gene Delivery. *J. Drug Deliv.* **2011**, 2011, 1–12. <https://doi.org/10.1155/2011/326497>.
- (19) HANDJANI-VILA, R. M.; RIBIER, A.; RONDOT, B.; VANLERBERGHIE, G. Dispersions of Lamellar Phases of Non-Ionic Lipids in Cosmetic Products. *Int. J. Cosmet. Sci.* **1979**, 1 (5), 303–314. <https://doi.org/10.1111/j.1467-2494.1979.tb00224.x>.
- (20) Vattulainen, I.; Rog, T. Lipid Simulations: A Perspective on Lipids in Action. *Cold Spring Harb. Perspect. Biol.* **2011**, 3 (4), 1–13. <https://doi.org/10.1101/cshperspect.a004655>.
- (21) Klein, M. L.; Shinoda, W. Large-Scale Molecular Dynamics Simulations of Self-Assembling Systems. *Science (80-.)*. **2008**, 321 (5890), 798–800. <https://doi.org/10.1126/science.1157834>.
- (22) Allen, D. T.; Lorenz, C. D. Molecular Scale Simulations of the Self-Assembly of Amphiphilic Molecules: Current State-of-the-Art and Future Directions. *J. Self-Assembly Mol. Electron.* **2015**, 2015 (1), 01–38. <https://doi.org/10.13052/jsame2245-4551.2015006>.
- (23) *Coarse-Graining of Condensed Phase and Biomolecular Systems*; Voith, G. A., Ed.; CRC Press: Boca Raton, 2008. <https://doi.org/10.1201/9781420059564>.
- (24) Brannigan, G.; Lin, L. C. L.; Brown, F. L. H. Implicit Solvent Simulation Models for Biomembranes. *Eur. Biophys. J.* **2006**, 35 (2), 104–124. <https://doi.org/10.1007/s00249-005-0013-y>.
- (25) Drouffe, J. M.; Maggs, A. C.; Leibler, S. Computer Simulations of Self-Assembled Membranes. *Science (80-.)*. **1991**, 254 (5036), 1353–1356. <https://doi.org/10.1126/science.1962193>.
- (26) Noguchi, H.; Takasu, M. Self-Assembly of Amphiphiles into Vesicles: A Brownian Dynamics Simulation. *Phys. Rev. E - Stat. Physics, Plasmas, Fluids, Relat. Interdiscip. Top.* **2001**, 64 (4), 7. <https://doi.org/10.1103/PhysRevE.64.041913>.
- (27) Farago, O. “Water-Free” Computer Model for Fluid Bilayer Membranes. *J. Chem. Phys.* **2003**, 119 (1), 596–605. <https://doi.org/10.1063/1.1578612>.
- (28) Brannigan, G.; Brown, F. L. H. Solvent-Free Simulations of Fluid Membrane Bilayers. *J. Chem. Phys.* **2004**, 120 (2), 1059–1071. <https://doi.org/10.1063/1.1625913>.
- (29) Wang, Z. J.; Frenkel, D. Modeling Flexible Amphiphilic Bilayers: A Solvent-Free off-Lattice Monte Carlo Study. *J. Chem. Phys.* **2005**, 122 (23). <https://doi.org/10.1063/1.1927509>.
- (30) Cooke, I. R.; Kremer, K.; Deserno, M. Tunable Generic Model for Fluid Bilayer Membranes. *Phys. Rev. E - Stat. Nonlinear, Soft Matter Phys.* **2005**, 72 (1), 2–5. <https://doi.org/10.1103/PhysRevE.72.011506>.
- (31) Cooke, I. R.; Deserno, M. Solvent-Free Model for Self-Assembling Fluid Bilayer Membranes: Stabilization of the Fluid Phase Based on Broad Attractive Tail Potentials. *J. Chem. Phys.* **2005**, 123 (22).

- <https://doi.org/10.1063/1.2135785>.
- (32) Noguchi, H. Solvent-Free Coarse-Grained Lipid Model for Large-Scale Simulations. *J. Chem. Phys.* **2011**, *134* (5), 0–12. <https://doi.org/10.1063/1.3541246>.
 - (33) Rand, R. P.; Parsegian, V. A. Hydration Forces between Phospholipid Bilayers. *Biochim. Biophys. Acta - Rev. Biomembr.* **1989**, *988* (3), 351–376. [https://doi.org/10.1016/0304-4157\(89\)90010-5](https://doi.org/10.1016/0304-4157(89)90010-5).
 - (34) Leckband, D.; Israelachvili, J. *Intermolecular Forces in Biology*; 2001; Vol. 34. <https://doi.org/10.1017/s0033583501003687>.
 - (35) Dey, S.; Saha, J. Solvent-Free, Molecular-Level Modeling of Self-Assembling Amphiphiles in Water. *Phys. Rev. E* **2017**, *95* (2), 023315. <https://doi.org/10.1103/PhysRevE.95.023315>.
 - (36) Dey, S.; Saha, J. Minimal Coarse-Grained Modeling toward Implicit Solvent Simulation of Generic Bolaamphiphiles. *J. Phys. Chem. B* **2020**, *124* (14), 2938–2949. <https://doi.org/10.1021/acs.jpcc.0c00734>.
 - (37) Sun, X.; Gezelter, J. D. Dipolar Ordering in the Ripple Phases of Molecular-Scale Models of Lipid Membranes. *J. Phys. Chem. B* **2008**, *112* (7), 1968–1975. <https://doi.org/10.1021/jp0762020>.
 - (38) Klauda, J. B.; Roberts, M. F.; Redfield, A. G.; Brooks, B. R.; Pastor, R. W. Rotation of Lipids in Membranes: Molecular Dynamics Simulation, 31P Spin-Lattice Relaxation, and Rigid-Body Dynamics. *Biophys. J.* **2008**, *94* (8), 3074–3083. <https://doi.org/10.1529/biophysj.107.121806>.
 - (39) Marsh, D. Molecular Motion in Phospholipid Bilayers in the Gel Phase: Long Axis Rotation. *Biochemistry* **1980**, *19* (8), 1632–1637. <https://doi.org/10.1021/bi00549a017>.
 - (40) Gay, J. G.; Berne, B. J. Modification of the Overlap Potential to Mimic a Linear Site-Site Potential. *J. Chem. Phys.* **1981**, *74* (6), 3316–3319. <https://doi.org/10.1063/1.441483>.
 - (41) Bates, M. A.; Luckhurst, G. R. Computer Simulation of Liquid Crystal Phases Formed by Gay-Berne Mesogens. In *Liquid Crystals I*; Springer Berlin Heidelberg: Berlin, Heidelberg, 1999; Vol. 94, pp 65–137. https://doi.org/10.1007/3-540-68305-4_3.
 - (42) Wilson, M. R. Molecular Simulation of Liquid Crystals: Progress towards a Better Understanding of Bulk Structure and the Prediction of Material Properties. *Chem. Soc. Rev.* **2007**, *36* (12), 1881–1888. <https://doi.org/10.1039/b612799c>.
 - (43) Allen, M. P. Molecular Simulation of Liquid Crystals. *Mol. Phys.* **2019**, *117* (18), 2391–2417. <https://doi.org/10.1080/00268976.2019.1612957>.
 - (44) Weeks, J. D.; Chandler, D.; Andersen, H. C. Role of Repulsive Forces in Determining the Equilibrium Structure of Simple Liquids. *J. Chem. Phys.* **1971**, *54* (12), 5237–5247. <https://doi.org/10.1063/1.1674820>.
 - (45) Heyes, D. M.; Okumura, H. Some Physical Properties of the Weeks–Chandler–Andersen Fluid. *Mol. Simul.* **2006**, *32* (1), 45–50. <https://doi.org/10.1080/08927020500529442>.
 - (46) Vega, C.; Lago, S. A Fast Algorithm to Evaluate the Shortest Distance between Rods. *Comput. Chem.* **1994**, *18* (1), 55–59. [https://doi.org/10.1016/0097-8485\(94\)80023-5](https://doi.org/10.1016/0097-8485(94)80023-5).
 - (47) Allen, M. P.; Germano, G. Expressions for Forces and Torques in Molecular Simulations Using Rigid Bodies. *Mol. Phys.* **2006**, *104* (20–21), 3225–3235. <https://doi.org/10.1080/00268970601075238>.
 - (48) Arnarez, C.; Uusitalo, J. J.; Masman, M. F.; Ingólfsson, H. I.; De Jong, D. H.; Melo, M. N.; Periole, X.; De Vries, A. H.; Marrink, S. J. Dry Martini, a Coarse-Grained Force Field for Lipid Membrane Simulations with Implicit Solvent. *J. Chem. Theory Comput.* **2015**, *11* (1), 260–275. <https://doi.org/10.1021/ct500477k>.
 - (49) Brannigan, G.; Philips, P. F.; Brown, F. L. H. Flexible Lipid Bilayers in Implicit Solvent. *Phys. Rev. E - Stat. Nonlinear, Soft Matter Phys.* **2005**, *72* (1), 4–7. <https://doi.org/10.1103/PhysRevE.72.011915>.
 - (50) Hoover, W. G. Canonical Dynamics: Equilibrium Phase-Space Distributions. *Phys. Rev. A* **1985**, *31* (3), 1695–1697. <https://doi.org/10.1103/PhysRevA.31.1695>.
 - (51) Nosé, S. An Extension of the Canonical Ensemble Molecular Dynamics Method. *Mol. Phys.* **1986**, *57* (1), 187–191. <https://doi.org/10.1080/00268978600100141>.
 - (52) Holian, B. L.; Voter, A. F.; Ravelo, R. Thermostatted Molecular Dynamics: How to Avoid the Toda Demon Hidden in Nosé-Hoover Dynamics. *Phys. Rev. E* **1995**, *52* (3), 2338–2347. <https://doi.org/10.1103/PhysRevE.52.2338>.
 - (53) Dey, S. Time-Reversible, Symplectic, Angular Velocity Based Integrator for Rigid Linear Molecules. **2018**. <https://arxiv.org/abs/1811.06450>.
 - (54) Dey, S. Minimal Modification to Nose-Hoover Barostat Enables Correct NPT Sampling. **2020**. <https://arxiv.org/abs/2007.01838>.
 - (55) Kunz, W.; Testard, F.; Zemb, T. Correspondence between Curvature, Packing Parameter, and Hydrophilic-Lipophilic Deviation Scales around the Phase-Inversion Temperature. *Langmuir* **2009**, *25* (1), 112–115. <https://doi.org/10.1021/la8028879>.
 - (56) Feller, S. E.; Pastor, R. W. Constant Surface Tension Simulations of Lipid Bilayers: The Sensitivity of Surface Areas and Compressibilities. *J. Chem. Phys.* **1999**, *111* (3), 1281–1287. <https://doi.org/10.1063/1.479313>.
 - (57) Jähnig, F. What Is the Surface Tension of a Lipid Bilayer Membrane? *Biophys. J.* **1996**, *71* (3), 1348–1349. [https://doi.org/10.1016/S0006-3495\(96\)79336-0](https://doi.org/10.1016/S0006-3495(96)79336-0).
 - (58) Allen, M. P.; Tildesley, D. J. *Computer Simulation of Liquids: Second Edition*; Oxford University Press, 2017; Vol. 1. <https://doi.org/10.1093/oso/9780198803195.001.0001>.
 - (59) Frenkel, D.; Smit, B. *Understanding Molecular Simulation*; Academic Press, 2002.
 - (60) Dimova, R. Recent Developments in the Field of Bending Rigidity Measurements on Membranes. *Adv. Colloid Interface Sci.* **2014**, *208*, 225–234. <https://doi.org/10.1016/j.cis.2014.03.003>.
 - (61) Johner, N.; Harries, D.; Khelashvili, G. Curvature and Lipid Packing Modulate the Elastic Properties of Lipid Assemblies: Comparing HII and Lamellar Phases. *J. Phys. Chem. Lett.* **2014**, *5* (23), 4201–4206. <https://doi.org/10.1021/jz5022284>.
 - (62) Doktorova, M.; Harries, D.; Khelashvili, G. Determination of Bending Rigidity and Tilt Modulus of Lipid Membranes from Real-Space Fluctuation Analysis of Molecular Dynamics Simulations. *Phys. Chem. Chem. Phys.* **2017**, *19* (25), 16806–16818. <https://doi.org/10.1039/C7CP01921A>.
 - (63) Johner, N.; Harries, D.; Khelashvili, G. Implementation of a Methodology for Determining Elastic Properties of Lipid Assemblies from Molecular Dynamics Simulations. *BMC Bioinformatics* **2016**, *17* (1), 1–11. <https://doi.org/10.1186/s12859-016-1003-z>.
 - (64) Sackmann, E. Physical Basis of Self-Organization and Function of Membranes: Physics of Vesicles. In *Handbook of Biological Physics*; Lipowsky, R., Sackmann, E., Eds.; 1995; Vol. 1, pp 213–304. [https://doi.org/10.1016/S1383-8121\(06\)80022-9](https://doi.org/10.1016/S1383-8121(06)80022-9).
 - (65) Rawicz, W.; Olbrich, K. C.; McIntosh, T.; Needham, D.; Evans, E. Effect of Chain Length and Unsaturation on Elasticity of Lipid Bilayers. *Biophys. J.* **2000**, *79* (1), 328–339. [https://doi.org/10.1016/S0006-3495\(00\)76295-3](https://doi.org/10.1016/S0006-3495(00)76295-3).
 - (66) Bloom, M.; Evans, E.; Mouritsen, O. G. Physical Properties of the Fluid Lipid-Bilayer Component of Cell Membranes: A Perspective. *Q. Rev. Biophys.* **1991**, *24* (3), 293–397. <https://doi.org/10.1017/S0033583500003735>.
 - (67) Goetz, R.; Gompper, G.; Lipowsky, R. Mobility and Elasticity of Self-Assembled Membranes. **1999**, 221–224.
 - (68) Marrink, S. J.; Mark, A. E. Effect of Undulations on Surface Tension in Simulated Bilayers. *J. Phys. Chem. B* **2001**, *105* (26), 6122–6127. <https://doi.org/10.1021/jp0103474>.

- (69) May, S. Trans-Monolayer Coupling of Fluid Domains in Lipid Bilayers. *Soft Matter* **2009**, *5* (17), 3148–3156. <https://doi.org/10.1039/b901647c>.
- (70) Risbo, J.; Sperotto, M. M.; Mouritsen, O. G. Theory of Phase Equilibria and Critical Mixing Points in Binary Lipid Bilayers. *J. Chem. Phys.* **1995**, *103* (9), 3643–3656. <https://doi.org/10.1063/1.470041>.
- (71) Jørgensen, K.; Sperotto, M. M.; Mouritsen, O. G.; Ipsen, J. H.; Zuckermann, M. J. Phase Equilibria and Local Structure in Binary Lipid Bilayers. *BBA - Biomembr.* **1993**, *1152* (1), 135–145. [https://doi.org/10.1016/0005-2736\(93\)90240-Z](https://doi.org/10.1016/0005-2736(93)90240-Z).
- (72) Wallace, E. J.; Hooper, N. M.; Olmsted, P. D. Effect of Hydrophobic Mismatch on Phase Behavior of Lipid Membranes. *Biophys. J.* **2006**, *90* (11), 4104–4118. <https://doi.org/10.1529/biophysj.105.062778>.
- (73) Knoll, W.; Schmidt, G.; Sackmann, E.; Ibel, K. Critical Demixing in Fluid Bilayers of Phospholipid Mixtures. A Neutron Diffraction Study. *J. Chem. Phys.* **1983**, *79* (7), 3439–3442. <https://doi.org/10.1063/1.446193>.
- (74) Fowler, P. W.; Williamson, J. J.; Sansom, M. S. P.; Olmsted, P. D. Roles of Interleaflet Coupling and Hydrophobic Mismatch in Lipid Membrane Phase-Separation Kinetics. *J. Am. Chem. Soc.* **2016**, *138* (36), 11633–11642. <https://doi.org/10.1021/jacs.6b04880>.
- (75) García-Sáez, A. J.; Chiantia, S.; Schuille, P. Effect of Line Tension on the Lateral Organization of Lipid Membranes. *J. Biol. Chem.* **2007**, *282* (46), 33537–33544. <https://doi.org/10.1074/jbc.M706162200>.
- (76) Cleaver, D. J.; Care, C. M.; Allen, M. P.; Neal, M. P. Extension and Generalization of the Gay-Berne Potential. *Phys. Rev. E - Stat. Physics, Plasmas, Fluids, Relat. Interdiscip. Top.* **1996**, *54* (1), 559–567. <https://doi.org/10.1103/PhysRevE.54.559>.
- (77) Fujimoto, T.; Parmryd, I. Interleaflet Coupling, Pinning, and Leaflet Asymmetry-Major Players in Plasma Membrane Nanodomain Formation. *Front. Cell Dev. Biol.* **2017**, *4* (JAN), 1–12. <https://doi.org/10.3389/fcell.2016.00155>.
- (78) Kuzmin, P. I.; Akimov, S. A.; Chizmadzhev, Y. A.; Zimmerberg, J.; Cohen, F. S. Line Tension and Interaction Energies of Membrane Rafts Calculated from Lipid Splay and Tilt. *Biophys. J.* **2005**, *88* (2), 1120–1133. <https://doi.org/10.1529/biophysj.104.048223>.
- (79) Gabriel, A. T.; Meyer, T.; Germano, G. Molecular Graphics of Convex Body Fluids. *J. Chem. Theory Comput.* **2008**, *4* (3), 468–476. <https://doi.org/10.1021/ct700192z>.
- (80) Sodt, A. J.; Head-Gordon, T. An Implicit Solvent Coarse-Grained Lipid Model with Correct Stress Profile. *J. Chem. Phys.* **2010**, *132* (20), 1–8. <https://doi.org/10.1063/1.3408285>.
- (81) Curtis, E. M.; Hall, C. K. Molecular Dynamics Simulations of DPPC Bilayers Using “LIME”, a New Coarse-Grained Model. *J. Phys. Chem. B* **2013**, *117* (17), 5019–5030. <https://doi.org/10.1021/jp309712b>.
- (82) Grime, J. M. A.; Madsen, J. J. Efficient Simulation of Tunable Lipid Assemblies Across Scales and Resolutions. **2019**.
- (83) Ionov, R.; Angelova, A. Swelling of Bilayer Lipid Membranes. *Thin Solid Films* **1996**, *284–285*, 809–812. [https://doi.org/10.1016/S0040-6090\(95\)08452-5](https://doi.org/10.1016/S0040-6090(95)08452-5).
- (84) Cooke, I. R.; Deserno, M. Coupling between Lipid Shape and Membrane Curvature. *Biophys. J.* **2006**, *91* (2), 487–495. <https://doi.org/10.1529/biophysj.105.078683>.

FIGURES

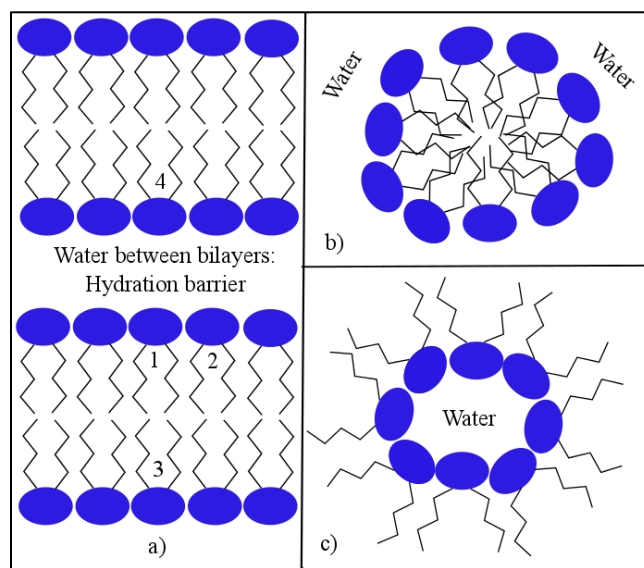


Figure 1. Schematic diagrams of lipid aggregates with different curvatures. Lipid cartoon: Blue – hydrophilic headgroup, Jagged lines – hydrophobic tails. a) Two hydrated bilayers separated by hydration force (No curvature); b) Cross-section of direct micelle (Positive curvature); c) Cross-section of inverted micelle (Negative curvature).

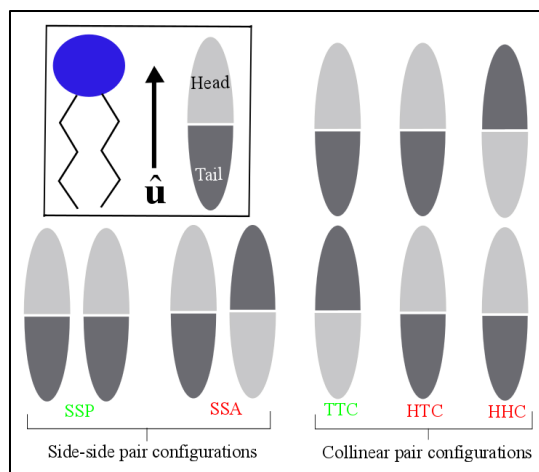


Figure 2. Inset: Lipid represented as a directed ellipsoid. Five canonical pair configurations— SSP: Side-Side Parallel, SSA: Side-Side Antiparallel, TTC: Tail-Tail Collinear, HTC: Head-Tail Collinear, HHC: Head-Head Collinear. Green ink denotes bound configuration (potential well-depth > 0); Red ink denotes unbound configuration (potential well-depth < 0).

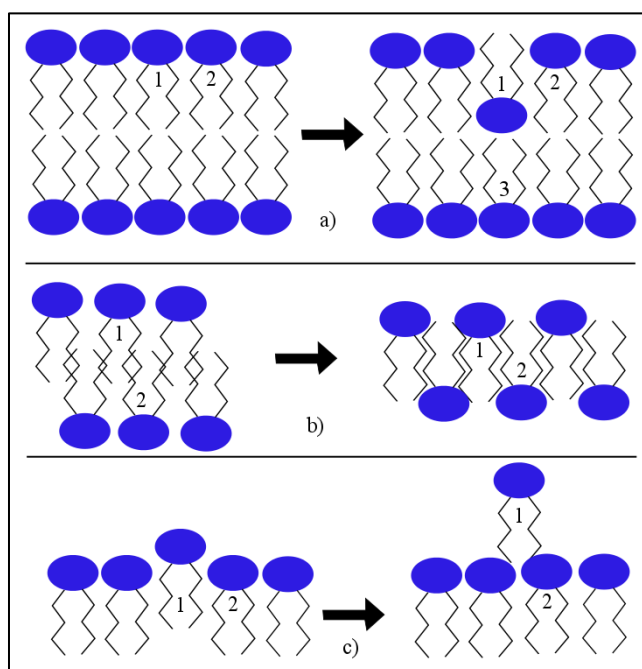


Figure 3. a) Lipid flip within a leaflet. The flipped lipid (1) forms SSA configuration with 2 and HTC with 3; b) Interdigitation between leaflets. Lipids 1 and 2 become SSA after interdigitation; c) Lipid protrusion from a leaflet. The protruded lipid (1) is almost HTC with 2.

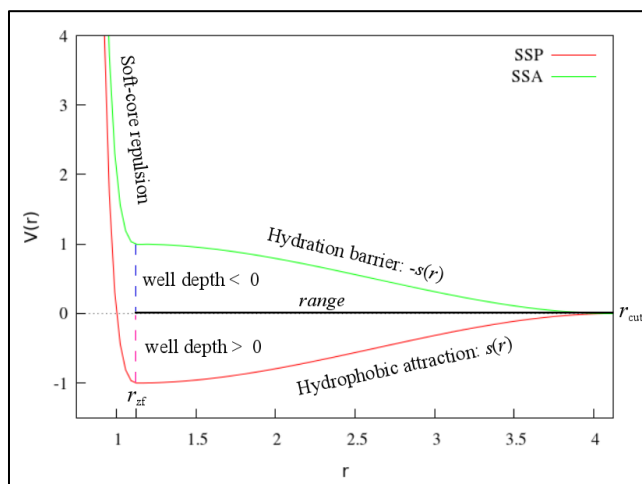


Figure 4. Potential energy between a pair of SiMPLISTIC lipids in SSP and SSA orientations as functions of their centre-centre distance, r . SSP must be stable and bound, hence the attractive tail of the potential. SSA must be unstable and unbound, hence the repulsive tail. Likewise, the TTC orientation has an attractive tail and each of the HTC and HHC orientations has a repulsive tail (not shown here).

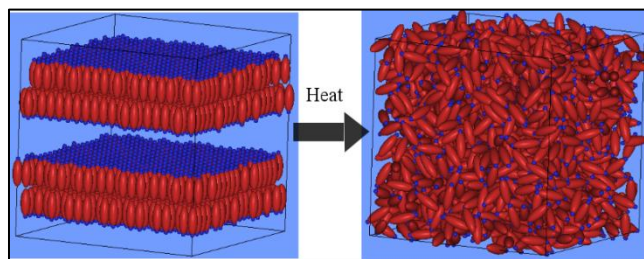


Figure 5. How the disordered, isotropic phase was prepared from preassembled lattice bilayers with sufficient interbilayer distance. SiMPLISTIC lipids are depicted as red spheroids with their head-ends marked with blue beads. The sky blue background implies the aqueous environment. This and other such renderings depicted in this work were performed using the molecular graphics software QMGA⁷⁹.

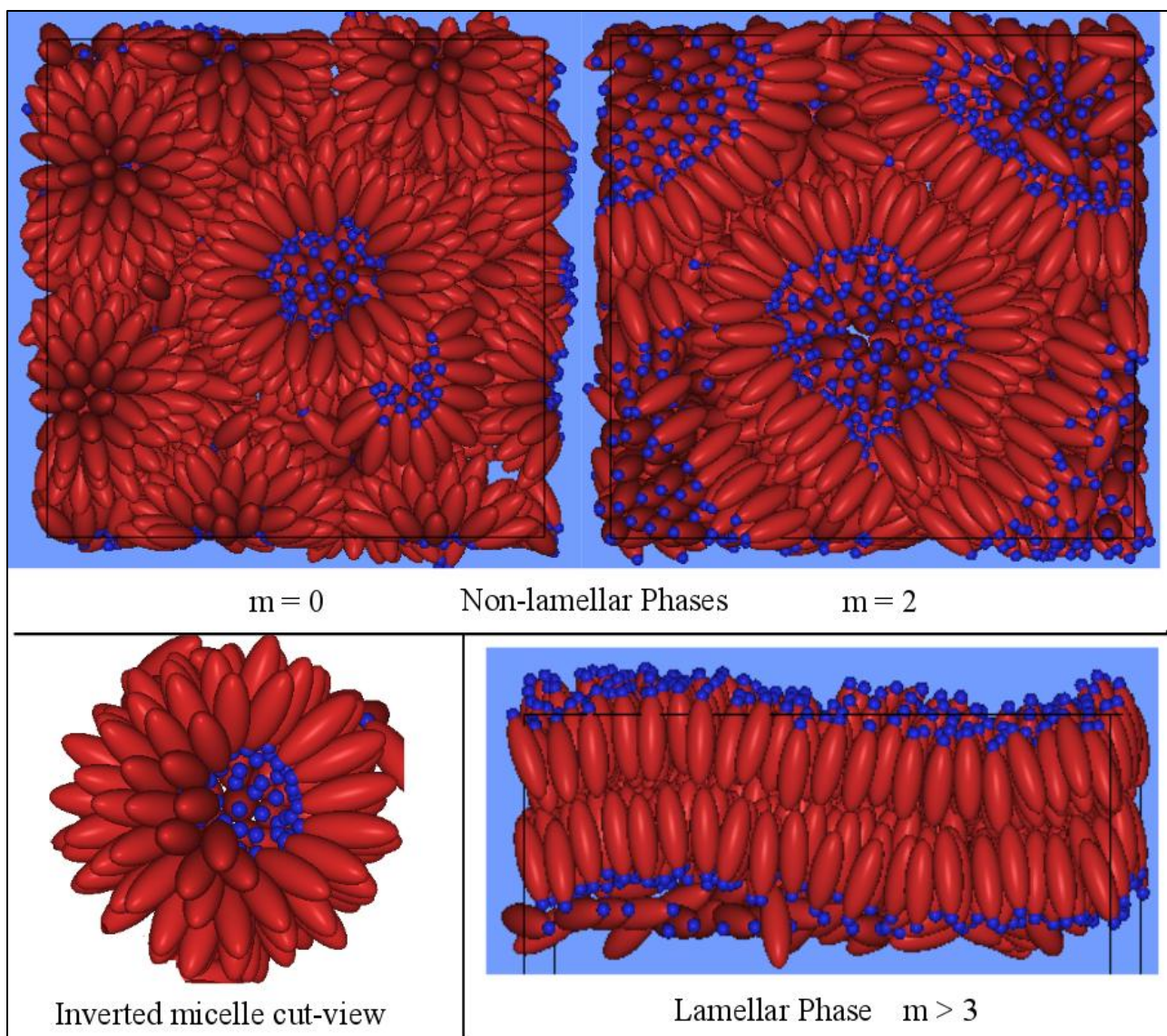


Figure 6. Self-assembled phases formed by SiMPLISTIC for different values of m . Lipids are depicted as red spheroids with their head-ends marked blue. The sky blue background implies the water environment. The non-lamellar phases are formed by closely packed inverted micelles (compare with the schematic cross-section in Figure 1). For enhanced clarity, a slice of an inverted micelle is also shown. The micellar radii are greater (and equivalently, the curvature is lesser) for $m = 2$ compared to $m = 0$. For $m > 3$ bilayers are obtained—a close-up of a box-spanning bilayer is shown [the stray lipids below the lower leaflet of the bilayer are actually part of a separate aggregate in the background (that we have sliced off for clarity) and do not belong to the bilayer in focus].

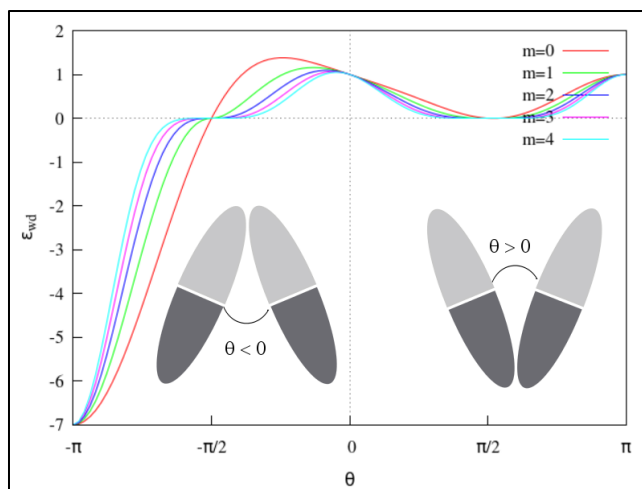


Figure 7. Well-depth ε_{wd} of the SiMPLISTIC potential as a function of the lipid splay angle θ for different values of m . The peak shifts towards $\theta=0$ for increasing m . Hence, increased m leads to a preference for decreased splay. It is easy to see from the spheroid configurations that packing pairs of lipids with $\theta < 0$ would generate inverted micelles (Figure 1c). Hence, the effective molecular shape (packing parameter) of lipids preferring $\theta < 0$ is similar to an inverted (truncated) cone.

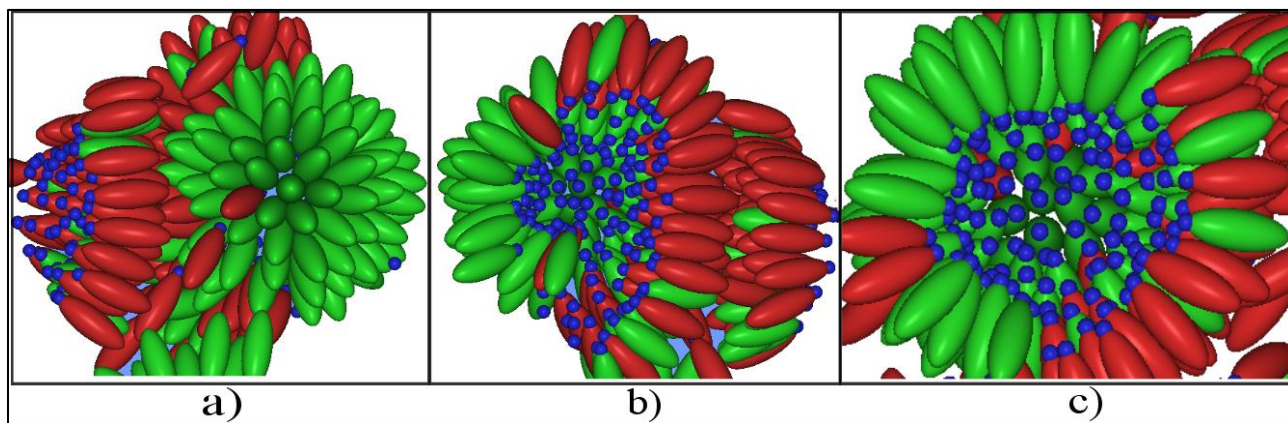


Figure 8. Close-ups of self-assembled phases generated by mixtures of two types of SiMPLISTIC lipids differing only in m . Red lipids have $m=4$ and green ones have $m=0$. Green lipids prefer inverted micelles (a), whereas red lipids prefer bilayer formation (b). Panel c shows the cross-section of an inverted micelle.

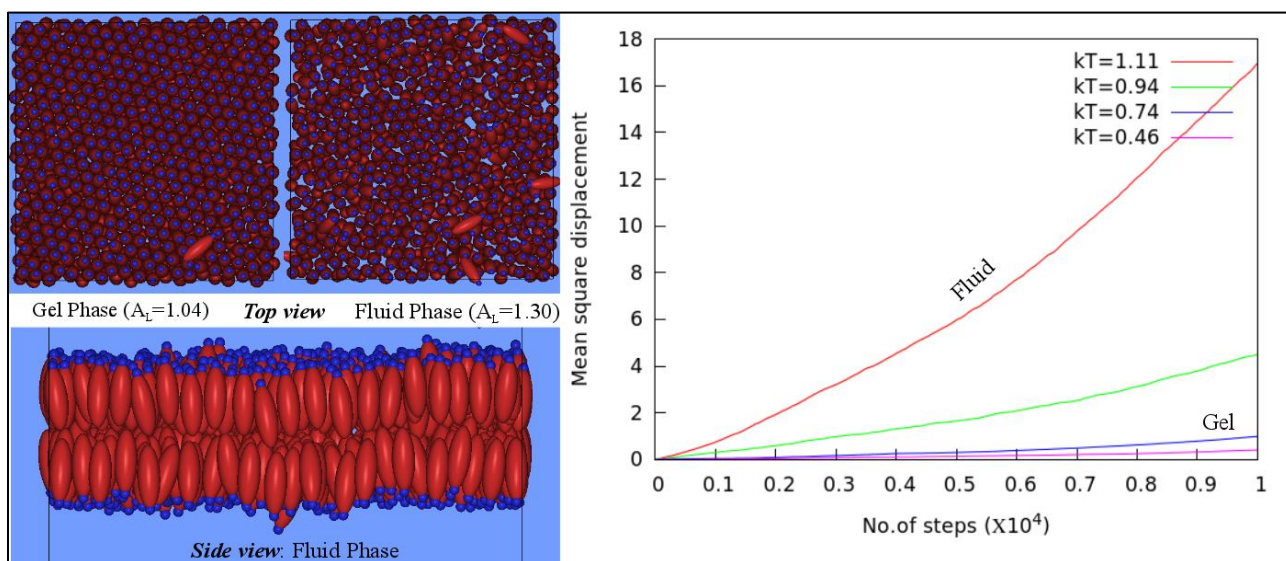


Figure 9. SiMPLISTIC shows fluid-gel transition in model membranes. The membrane phase can be deduced from the mean square displacements, and the order of lipid arrangement in the leaflets. Lipids in the fluid phase are much more diffusive but much less ordered and less densely packed (hence, the greater area per lipid, A_L). Note that no interdigitation or tilt is apparent in the side view. Units: kT in ε_0 and A_L in σ_0^2 .

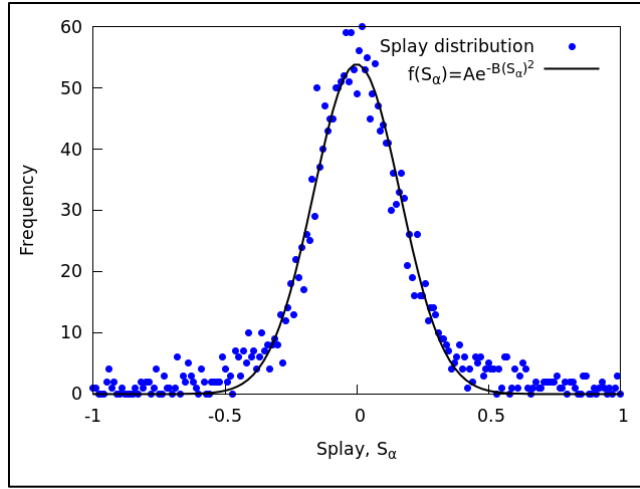


Figure 10. A Gaussian with zero mean fitted to the frequency distribution of splay obtained from a tensionless membrane at temperature, $kT = 1.11\epsilon_0$. An estimate for the membrane bending modulus κ_C can be obtained from the fit as $\kappa_C = 2BkT/A_L$, where A_L is the area per lipid.

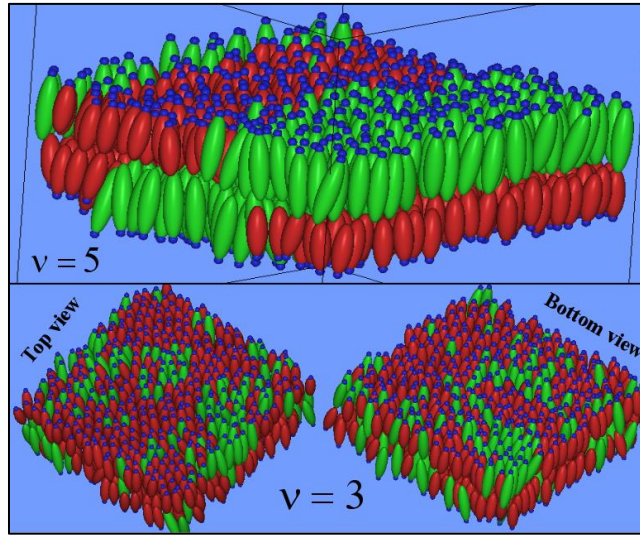


Figure 11. Hydrophobic mismatch driven demixing of SiMPLISTIC lipids at temperature, $kT = \epsilon_0$. Red and green lipids differ only in their spheroidal lengths (σ_e). Red: $\sigma_e = 3\sigma_0$, Green: $\sigma_e = 4\sigma_0$. For $\nu = 3$, the number ratio of red to green is 3:1. For $\nu = 5$, the number ratio is 1:1. Although clustering of lipids of the same color in each leaflet is clearly visible for both values of ν , a much cleaner phase separation occurs at $\nu = 5$ due to an increased line tension. Note that there is no domain registration between the leaflets.